Extension of the Lennard-Jones potential: Theoretical investigations into rare-gas clusters and crystal lattices of He, Ne, Ar, and Kr using many-body interaction expansions

Peter Schwerdtfeger,* Nicola Gaston, and Robert P. Krawczyk
Theoretical and Computational Chemistry Research Centre, Building 44, Institute of Fundamental Sciences, Massey University (Albany Campus), Private Bag 102904, North Shore MSC, Auckland, New Zealand

Ralf Tonner
Fachbereich Chemie, Philipps-Universität Marburg, Hans-Meerwein-Strasse, 35032 Marburg, Germany

Gloria E. Moyano
Research School of Chemistry, Australian National University, Canberra, A.C.T. 0200, Australia
(Received 14 August 2005; revised manuscript received 9 November 2005; published 21 February 2006)

The many-body expansion $V_{\text{int}}=\Sigma_{i<j}V^{(2)}(r_{ij})+\Sigma_{i<j<k}V^{(3)}(r_{ij},r_{ik},r_{jk})+\cdots$, in terms of interaction potentials between rare-gas atoms converges fast at distances $r>r_{HS}$, with r_{HS} being the hard-sphere radius at the start of the repulsive wall of the interaction potential. Hence, for the solid state where the minimum distance is always above r_{HS}, a reasonable accuracy is already obtained for the lattice parameters and cohesive energies of the rare-gas elements using precise two-body terms. All tested two-body potentials show a preference of the hcp over the fcc structure. We demonstrate that this is always the case for the Lennard-Jones potential. We extend the Lennard-Jones potential to obtain analytical expressions for the lattice parameters, cohesive energy, and bulk modulus using the solid-state parameters of Lennard-Jones and Ingham [Proc. R. Soc. London, Ser. A **107**, 636 (1925)], which we evaluate up to computer precision for the cubic lattices and hcp. The inclusion of three-body terms does not change the preference of hcp over fcc, and zero-point vibrational effects are responsible for the transition from hcp to fcc as shown recently by Rosciszewski *et al.* [Phys. Rev. B **62**, 5482 (2000)]. More precisely, we show that it is the coupling between the harmonic modes which leads to the preference of fcc over hcp, as the simple Einstein approximation of moving an atom in the static field of all other atoms fails to describe this difference accurately. Anharmonicity corrections to the crystal stability are found to be small for argon and krypton. We show that at pressures higher than 15 GPa three-body effects become very important for argon and good agreement is reached with experimental high-pressure density measurements up to 30 GPa, where higher than three-body effects become important. At high pressures we find that fcc is preferred over the hcp structure. Zero-point vibrational effects for the solid can be successfully estimated from an extrapolation of the cluster zero-point vibrational energies with increasing cluster size *N*. For He, the harmonic zero-point vibrational energy is predicted to be always above the potential energy contribution for all cluster sizes up to the solid state at structures obtained from the two-body force. Here anharmonicity effects are very large which is typical for a quantum solid.

DOI: 10.1103/PhysRevB.73.064112 PACS number(s): 61.50.Ah, 63.20.−e, 63.22.+m, 71.15.Nc

I. INTRODUCTION

Elemental rare-gas clusters are known to be as typical examples of Lennard-Jones (LJ) systems.[1–7] However, when considering the solid, the periodic LJ crystal is predicted to have a hexagonal close-packed (hcp) structure,[8,9] while the experimentally determined structures for the Ne, Ar, and Kr crystals are all face centered cubic (fcc).[10] That discrepancy, known as the rare-gas solid (RGS) problem,[11] has led to an intense debate about the growth process of such clusters, as well as on the effects accounting for the difference in the predicted energies of the fcc and hcp lattices.[12] Although this difference is actually much smaller than originally anticipated,[13,14] it is decisive and has stimulated much theoretical research on the interactions between rare-gas atoms.[2]

The most accurate computational quantum methods available are required for describing weak interactions between rare-gas atoms, either in the cluster or in the solid, which currently is a formidable task. Even for the simple diatomic system both electron correlation and relativistic effects for the heavier elements have to be taken into account. Density functional theory is currently not capable of accurately describing van der Waals–type clusters,[15] even though improvements are underway.[16–19] For the solid similar problems remain and it is not straightforward to describe electron correlation for van der Waals solids.

In order to perform global structure optimizations for larger rare-gas clusters and to establish property trends with increasing cluster size *N*, we need an affordable but accurate approach. Relativistic *ab initio* electronic structure calculations including electron correlation are possible only for the smallest clusters. Furthermore, the number of local minima for clusters increases exponentially with *N* and it is nontrivial to find the global minimum.[20] A useful strategy to study the most stable structures of rare-gas clusters and the convergence towards the bulk could use a truncated expansion of the many-body interaction potential energy derived from accurate *ab initio* theory,

$$V_{\mathrm{int}}(N) = \sum_n V^{(n)}(N) = \sum_{i<j}^{N} V^{(2)}(r_{ij}) + \sum_{i<j<k}^{N} V^{(3)}(r_{ij}, r_{ik}, r_{jk}) + \cdots . \quad (1)$$

Once the structures are obtained, single-point relativistic *ab initio* or density functional calculations can be used to determine certain electronic properties. For the total electronic energy, expansions like Eq. (1) converge smoothly only in the long range—that is for van der Waals clusters—and the short-range behavior for systems under high pressure is not accurately known.[21]

Concerning the solid state of Ne through Xe, recent *ab initio* coupled-cluster calculations by Rosciszewski *et al.*[14,22,23] of cohesive energies point towards the zero-point vibrational energy (ZPVE) as the main reason responsible for the stabilization of the fcc over the hcp structure, followed by a much smaller contribution from short-range three-body terms, as already suggested in 1955 by Barron and Domb[24] and later by Niebel and Venables.[25] Jansen,[13,26] Richardson and Mahanty,[27] and more recently Lotrich and Szalewicz[12] argued, however, that already the three-body forces lead to fcc being preferred over hcp. These three-body effects are important as two-body potentials significantly overestimate the cohesive energies of rare-gas crystals—i.e., between 32% and 40% for Ne to about 12%–13% for Xe.[13,22] In comparison, ZPVE corrections amount to 28% of the cohesive energy for Ne and only 3% for Xe.[14] We mention that (quartic) anharmonicity corrections were also used to explain the stability of the fcc over the hcp phase.[28]

Further insight into the stability of the two-phase problem can be gained by studying the nucleation process of rare-gas clusters. Valuable clues about the structural trends or the crystal growth process are obtained by combining information from experiments and prototype cluster simulations. Mass spectra in free-jet expansions of neutral rare-gas clusters have provided the magic numbers[29,30]—i.e., specific sizes related to prominent stabilities (see, e.g., review by Kumar[6] and references cited therein). For the small-N range those numbers are in closer agreement with the Mackay icosahedral shell clusters than with other structural types (like fcc). Therefore, icosahedral packing seems to be the basic growth pattern for small cluster sizes, with strong experimental support for the cases of xenon and argon.[29–31] Furthermore, global minima for the LJ clusters, which are known for nearly all sizes below $N \sim 560$,[32,33] follow the icosahedral growth pattern with few exceptions, a trend that may continue for much bigger sizes.[3] However, the periodic solid cannot contain a fivefold symmetry axis characteristic of icosahedral clusters. Another problem is that with the simple LJ potential one may not get the expected fcc structure at medium to large cluster size,[7,34] so that the LJ model may become a rather poor approximation for rare-gas clusters when we are interested in structural trends towards the bulk limit.

Different hypotheses about the cluster growth have been proposed. For example, it was suggested that one or more transitions may lead from the icosahedral to fcc structures at high-N ranges.[31] However, research on diffraction patterns of argon clusters has shown that such a noncrystalline to crystalline transition is elusive and that large-size clusters ($10^3 < N < 10^5$) contain in fact a mixture of hcp, fcc, and random close-packed (rcp) regions, with no preference or trend towards the bulk structure,[34] contradicting the evolution of observed diffraction patterns for small-size clusters ($50 < N < 70$).[31] At the same time, other diffraction studies[35,36] for medium-size clusters ($N \sim 2000$) of argon and krypton are taken as evidence of the hypotheses of the coalescence of icosahedral clusters, which results in the formation of fcc regions with lattice defects, promoters of rapid fcc crystal growth.[37,38] Some alternative ideas could as well serve as a basis for a better understanding of this complex situation: the fcc crystal growth could be completely disconnected from the icosahedral cluster growth, or the structural trends and transitions could be temperature dependent.[39,40] Moreover, factors other than the precise form of the interaction potential could be crucial for the structural transitions of these clusters.[34]

Helium clusters and the solid state are often considered apart from the mentioned rare-gas studies because of their particular delocalized nature. Ground-state calculations for the nuclear Hamiltonian of small elemental rare-gas clusters[1] illustrate that, unlike in the cases of neon and argon, probability distribution functions for the bond lengths, bond angles, and dihedral angles of helium clusters are so broad, without the multiple peaks found in the classical clusters, that the helium clusters cannot be said to be arranged in any type of rigid geometry. The ZPVE energy for helium clusters is predicted to be comparable to the potential depth, and the average kinetic energy should be of the same order as the potential energy.[1] As a consequence, helium becomes solid at low temperatures only at pressures of greater than 2.5 kPa.[41] However, from recent diffraction studies there is some evidence for magic numbers in helium clusters.[42] We mention that quantum delocalization effects are not small in rare-gas clusters of elements other than helium.[43,44]

Considering that pair interactions account for most of the binding energy of the rare-gas clusters and subsequently for the cohesive energy of the RGS, the use of two-body potentials more accurate than the LJ appears as an important attempt towards the improvement of structure calculations of rare-gas clusters and the solid state. This is one of the main aspects studied in this paper for clusters R_N (R=Ne, Ar, and Kr; $N \leqslant 150$), along with the analysis of structural trends with the increasing size towards the bulk structure.

II. COMPUTATIONAL DETAILS

The potential energy for the clusters as well as for the lattices is expressed as a sum of two-body interatomic potentials $V^{(2)}(r)$, which come from accurate pointwise *ab initio* calculations for the systems He_2,[45] Ne_2,[46] Ar_2,[46] and Kr_2.[47] The data points for those potential curves were fitted to an extended LJ-type (ELJ) potential

$$V^{(2)}_{ELJ}(r) = \sum_{i=1}^{6} c_{2i+4} r^{-2i-4} \quad (2)$$

by a linear least-squares procedure, so that the fitting parameters c_{2i+4} for every dimer are given in Table I. Note that for

TABLE I. Fitting parameters for the two-body potentials of the rare gases from He to Kr according to Eq. (2). The parameters c_i are given in a.u. Equilibrium distance r_{min} and hard-sphere radius r_{HS} are in Å, and minimum energy V_{min} in cm^{-1} of the potential energy curve. The data for the fit procedure are taken from Refs. 45–47.

	He	Ne	Ar	Kr
c_6	0.51935577676634	−10.5097942564988	−123.635101619510	−227.476410584751
c_8	−313.906518089779	989.725135614556	21262.8963716972	50281.6033768459
c_{10}	11045.2101976432	−101383.865938807	−3239750.64086661	−9549691.98083359
c_{12}	−88571.2026084401	3918846.12841668	189367623.844691	658170535.750904
c_{14}	88684.2761441023	−56234083.4334278	−4304257347.72069	−17524714507.3525
c_{16}	946830.190858721	288738837.441765	35315085074.3605	166980981478.238
r_{min}	3.0503	3.0985	3.7782	4.0505
r_{HS}	2.7022	2.7700	3.3730	3.6161
V_{min}	−7.430	−28.62	−96.97	−135.4

the last coefficient we require that $c_{16}>0$ in order to obtain the correct repulsive behavior at small internuclear distances. We also carefully checked the roots of potential (2), which, beside the hard-sphere radius r_{HS} where the potential curve becomes repulsive, has no other physical solutions. Note that the coefficients c_{2i+4} do not correspond to the well-known van der Waals coefficients describing the long-range behavior of two interacting systems as the repulsive wall is automatically built in. Figure 1 shows the individual r^n contributions for Ar. It clearly demonstrates that all powers in Eq. (2) contribute significantly to the potential, from the short- to the long-range region. The rather divergent behavior at short range is probably the reason why such an expansion is not applied for the repulsive region; however, the usefulness of this ansatz will become apparent for solid-state properties.

We briefly discuss ansatz (2), which avoids artificially large interaction terms at long distances, leading to divergencies for the solid state. In order to make this point more transparent we assume the more general ansatz

$$V_{ELJ}^{(2)}(r) = \sum_{i=n_{\min}}^{n_{\max}} c_i r^{-i}. \tag{3}$$

We define this new potential as ELJ($n_{min}, n_{max}, \Delta n$) where the numbers in parentheses denote the minimum n_{min} and maximum n_{max} exponent in r^{-n} and the last number the increment Δn for the exponent. Here we use a ELJ(6,16,2) potential according to Eq. (1). This ansatz includes both the Lennard-Jones (6–12) potential,[48] ELJ(6,12,6), and the (more historical) Kratzer potential ELJ(1,2,1).[49] Consider the interaction of an atom sitting at the origin with an infinite number of equally spaced (by Δr) atoms along a single line on the positive x axis. We then get, for the total interaction energy per atom (which translates to the cohesive energy for the solid state) according to Eq. (3),

$$\begin{aligned} V_{int} &= \lim_{N\to\infty} \frac{1}{2}\sum_{n=1}^{N} V_{ELJ}^{(2)}(r_{0n}) \\ &\overset{r_{0n}=n\Delta r}{=} \lim_{N\to\infty} \frac{1}{2}\sum_{i=1}^{i_{max}} c_i \sum_{n=1}^{N} (n\Delta r)^{-i} \\ &= \frac{1}{2}\sum_{i=1}^{i_{max}} c_i \Delta r^{-i} \lim_{N\to\infty} \sum_{n=1}^{N} n^{-i}. \end{aligned} \tag{4}$$

We know that $\Sigma_{n=1}^{N} n^{-1} \to \infty$ $(N\to\infty)$ and r^{-1} terms in Eq. (3) should therefore not be used. Moreover, as shown in the Appendix, for a three-dimensional lattice, r^{-n} terms with $n \leqslant 3$ lead to a divergent series for the cohesive energy. Hence we conclude that one has to take great care of the correct long-range behavior in solid-state calculations or when dealing with larger clusters.

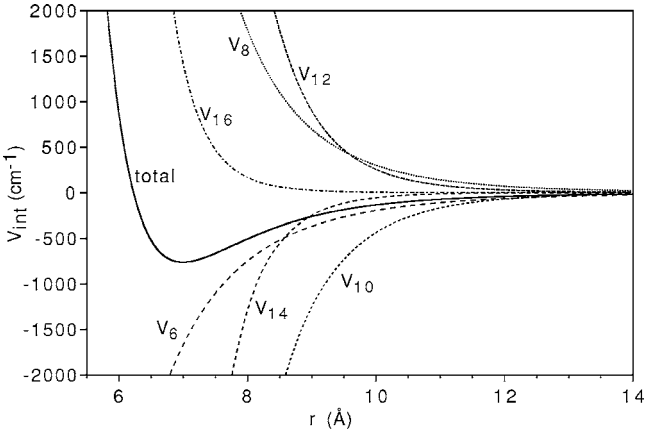

FIG. 1. Individual contributions for the ELJ(6,16,2) potential $V_{2i+4}(r)=c_{2i+4}r^{-2i-4}$ to the total interaction potential for Ar.

The minimum distances and energies obtained from the parameter fit in Eq. (2) agree with the original data to high accuracy. For example, for Ne_2 the data given by Cybulski and Toczylowski[46] of $r_e=3.0988$ Å and $E_{min}=28.604$ cm^{-1} are in perfect agreement with the data given in Table I. Global geometry optimizations were performed for all the clusters up to $N=150$ using a simulated annealing approach[50] together with a conjugate gradient local optimization routine to refine the optimization[50] as incorporated in our cluster structure program MAMBO.[51] The optimized geometries for the elemental rare-gas clusters were all true minima, established through a vibrational analysis. Symmetry groups of the optimal configurations corresponded with few exceptions to those of the typical LJ clusters. As He is a quantum liquid (solid), dynamic effects have to be included. Nevertheless,

we chose to include He for comparison here with the other rare-gas systems.

The adjusted potentials were tested in solid-state calculations together with other known two-body potentials using our program system SAMBA.[52] Optimization of the lattice parameters and calculation of the cohesive energies for homoatomic arrangements corresponding to sections of fcc, hcp, and bcc crystals were performed using numerical gradient procedures. Two different ways of calculating the cohesive energy are implemented in SAMBA, the first through a fast convergency expansion which makes use of the translational symmetry (T) of the Bravais lattice and does not contain the high-energy surface terms,

$$V_{\mathrm{int}}^{T}(N) = \frac{1}{2}\sum_{i} V^{(2)}(r_{0i}) + \frac{1}{3}\sum_{i<j} V^{(3)}(r_{0i}, r_{0j}, r_{ij}) + \cdots, \quad (5)$$

where r_{0i} is the distance between the inner most (central atom) and atom i, and the second by explicit evaluation of the many-body expansion (1). Both formulas (1) and (5) are identical in the limit of the solid state; that is, the cohesive energy is

$$E_{coh} = -\lim_{N\to\infty} V_{\mathrm{int}}^{T}(N) = -\lim_{N\to\infty} \frac{1}{N} V_{\mathrm{int}}(N). \quad (6)$$

For all the rare-gas elements considered in this work, the two expansions (1) and (5) were truncated at the two-body term. The initial values of the lattice parameters for the optimizations were taken from experimental reference data,[53] and the number of atoms N in the lattices was chosen to be $N \sim 100\,000$ atoms for the SAMBA program which gives an accuracy of $<10^{-1}$ cm^{-1} in the cohesive energy and $<10^{-4}$ Å in the lattice parameters for Ar; see Fig. 2. Even with 10 000 atoms the lattice parameters are converged to four significant figures. The difference between the fcc and hcp structures is however, very small for the rare gases—i.e., $<10^{-1}$ cm^{-1}—and therefore is below the converged cohesive energy at this cluster size. For this purpose, ansatz (2) will become very useful. Nevertheless, in taking care of using approximately the same number of atoms, N, for one specific atom for all crystal structures, this difference can be calculated to much higher accuracy.

For the zero-point vibrational energy of the solid we considered two-body forces only. From Eq. (1) we obtain the following force field for the two-body potential only:

$$\frac{\partial^2 V_{\mathrm{int}}}{\partial X_k \partial Y_k} = \sum_{i\neq k}^{N} \frac{\partial^2 V^{(2)}(r_{ik})}{\partial X_k \partial Y_k}, \quad \frac{\partial^2 V_{\mathrm{int}}}{\partial X_k \partial Y_j} = \frac{\partial^2 V^{(2)}(r_{kj})}{\partial X_k \partial Y_j} \quad \text{for } k \neq j, \quad (7)$$

where X_k and Y_j stand for the three Cartesian coordinates of atoms k and j. We chose N_{vib}=5000 atoms spherically embedded in more than 200 000 atoms and diagonalized the mass-weighted force field F_{ij} to obtain harmonic phonons in r space for the bcc, fcc, and hcp structures. For the numerical determination of the force field a step size of 10^{-3} a.u. was chosen for the atom displacements. For the (3,3)-block-diagonal elements in F_{ij}, translational symmetry was strictly applied to avoid surface effects. The most expensive part of these calculations is the diagonalization of the symmetric force field matrices of the size $(3N_{vib}, 3N_{vib})$. A Householder transformation was used, which is $\sim N_{vib}^3$ in CPU time. Diagonalization of the (3,3)-block-diagonal matrix gives directly the Einstein frequency. We mention that the hcp lattice consists of two hexagonal Bravais lattices and there are therefore two nonidentical atoms in the lattice. However, the Einstein frequencies for both type of atoms are identical.

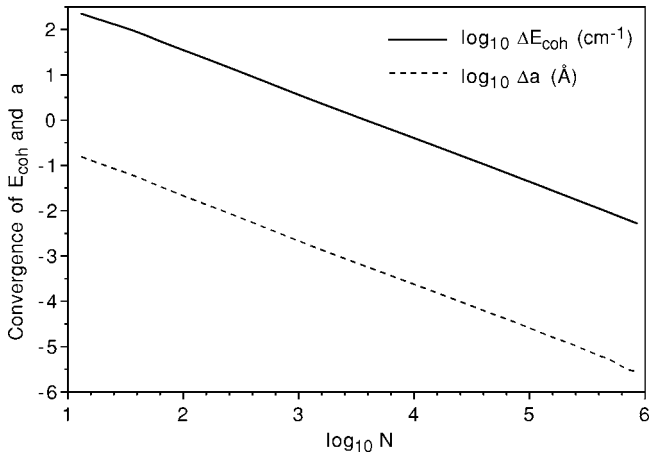

FIG. 2. Convergence of the cohesive energy E_{coh} (in cm^{-1}) and the lattice constant a (in Å) for fcc Ar using the Lennard-Jones potential of Ref. 79, shown on a logarithmic scale. $\Delta E_{coh} = -[E_{coh}(N) - E_{coh}(\infty)]$, where $E_{coh}(\infty)$ is obtained directly from Eq. (13). Similarily we have $\Delta a = a(N) - a(\infty)$.

Anharmonicity effects are only considered within the Einstein approximation by first-order perturbation theory—that is, by moving one atom in the field of all other atoms in the solid. Here only the even powers in Cartesian derivatives for the anharmonic force constants need to be included—namely, F_{iiii} and F_{iijj}, where i and j stands for the Cartesian coordinates X, Y, and Z of one atom in the solid. This only gives a rough estimate of anharmonicity effects as higher-order perturbation theory in a fully coupled mode analysis would be necessary to obtain accurate results, which currently is a nontrivial task. We note, however, that the F_{iijj} quartic force constants are as important as the corresponding F_{iiii} terms and cannot be neglected as done, for example, in a recent analysis of anharmonicity effects.[12]

For Ar we also considered three-body interactions by using the three-body ansatz of Lotrich and Szalewicz as described in detail in Ref. 12. Here we restrict the calculations for the three-body part to $N \sim 50\,000$ atoms, because these calculations scale like N^2 in computer time. For this solid the influence of the zero-point vibrational energy on the fcc and hcp lattice parameters and cohesive energies was also considered in more detail.

For the n-body decomposition of the rare-gas hexamers He_6, Ne_6, and Ar_6 we carried out scalar relativistic coupled-cluster [CCSD(T)] calculations using the Douglas-Kroll operator.[54,55] For the heaviest system in this series, Kr_6, coupled-cluster calculations became too consuming in computer time and we used second-order many-body perturbation theory instead (MBPT2). The basis sets used are cc-pVQZ-DK-Dunning sets[56–58] with the g and h functions

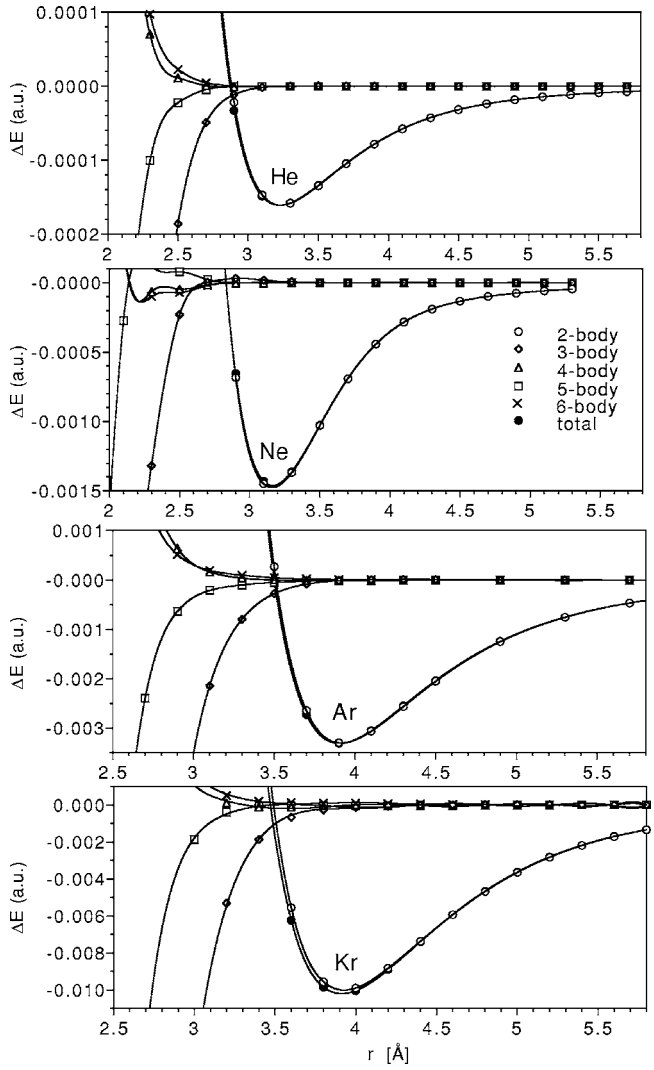

FIG. 3. Total n-body contributions to the rare-gas octahedron R_6 according to Eq. (1) as a function of the nearest-neighbor distance r. The total value is the sum of all n-body contributions.

removed. The two-body term is corrected for the basis-set superposition error using the method of Boys and Bernardi.[59]

III. RESULTS AND DISCUSSION

A. Convergence of the n-body interaction potential expansion

In order to discuss the convergence of the n-body expansion with increasing expansion parameter n of Eq. (1) we carried out CCSD(T) calculations for the octahedral arrangement R_6 from He up to Kr at different next-neighbor distances r. The second larger distance $r' > r$ in the octahedron is given by $r' = \sqrt{2}r$. The results are shown in Fig. 3 for He to Kr.

Since the equilibrium bond distances do not alter much from the smallest cluster to the solid state for rare-gas systems (compare r_{min} in Table I with the solid-state distances $r_{\min}^{SS}$ given in Table II), a reasonable description of the interaction potential under normal conditions is already obtained by using two-body potentials only.[60,61] This is very much a special feature of the rare-gas atoms,[62] as other closed-shell systems like mercury[63] or the alkaline-earth metals[62] show very large many-body effects becoming important already at small cluster sizes at distances close to the equilibrium distance, and for such systems the solid state cannot be described accurately anymore by restricting the interaction to a two-body potential only. However, it is evident that higher than two order terms in Eq. (1) become important close to the point where the repulsive region of the potential curve starts. Here the convergence of the n-body expansion becomes worse, and the use of the two-body term only may not be sufficient anymore for studies of rare-gas systems under high pressure. There is already experimental evidence for the importance of higher-body corrections from high-pressure studies of argon.[64] For intermolecular interactions between hydrogen molecules the importance of three-body forces was pointed out much earlier.[65] Figure 4 describes this situation nicely by showing the sum of three- to six-body terms in energy units of the binding energy E_b for scaled distances r/r_e. We also see that in the long-range region the sum of higher-order effects $(n>2)$ is repulsive, while it becomes attractive at shorter distances. These repulsive long-range effects are well known from Axilrod-Teller type of interactions and lead to equilibrium bond distances, for example, for argon of $r_e(\mathrm{Ar}_3) = 3.7812\ \text{Å} > r_e(\mathrm{Ar}_2) = 3.7782\ \text{Å}$ using the Cybulski-Toczylowski two-body potential[46] and the Lotrich-Szalewicz three-body potential.[12]

B. Two-body interaction potential and the solid state

Since we are not interested in the repulsive region of the potential surface, we restrict our study mainly to accurate two-body interactions as described in the computational section. We used the functional form of the two-body interaction potential as defined in Eq. (2). The parameters are listed in Table I, and the solid-state results are shown in Table II. We also used other two-body potentials published for He,[66,67] Ne,[68–71] Ar,[72–75] and Kr,[76–78] for comparison, including the well-known Lennard-Jones potential.[79] Helium is used only for comparison, as solid helium does not exist at normal pressure. There are a few potentials available for Xe which are included in our analysis. Table III shows the bulk moduli for the experimentally observed fcc lattice where we used the expression

$$B = \frac{1}{9cr_{min}^{SS}} \frac{\partial^2 V_{int}}{(\partial r^{SS})^2}\bigg|_{r_{min}^{SS}}, \tag{8}$$

where r_{min}^{SS} is the smallest minimum distance in the solid and c is a constant for the volume determination, $V = c(r_{min}^{SS})^3$, depending on the symmetry of the lattice. B is obtained numerically by changing the lattice parameters using a step size of 10^{-3} a.u.

Not surprisingly,[2] all calculations predict the fcc lattice to be very close in energy to the hcp one, with the hcp structure to be the global minimum for two-body potentials neglecting the ZPVE contribution. For comparison we also include the bcc structures, which are much higher in energy. With a few exceptions, all two-body potentials give similar results for

TABLE II. Minimum solid-state distance $r_{\min}^{SS}$, lattice parameters a, b, and c, and cohesive energies E_{coh} (not corrected for zero-point vibrational effects) for various two-body potentials obtained from a numerical optimization procedure.[a]

Element	Potential	Ref.	Structure	r_{min}^{SS}	$a=b$	c	E_{coh}
He	SFR[b]	45	hcp	2.9787	2.9791	4.8638	56.030
			fcc	2.9789	4.2128	4.2128	56.022
			bcc	2.9143	3.3652	3.3652	53.737
	PD	66	hcp	2.9662	2.9664	4.8435	53.571
			fcc	2.9663	4.1950	4.1950	53.565
			bcc	2.9034	3.3525	3.3525	51.293
	JA	67	hcp	2.8956	2.8959	4.7282	61.412
			fcc	2.8958	4.0953	4.0953	61.404
			bcc	2.8340	3.2725	3.2725	58.626
	LJ	79	hcp	2.8670	2.8673	4.6816	64.634
			fcc	2.8672	4.0548	4.0548	64.627
			bcc	2.8100	3.2447	3.2447	61.830
Ne	CT[b]	46	hcp	3.0336	3.0339	4.9535	226.728
			fcc	3.0338	4.2904	4.2904	226.706
			bcc	2.9715	3.4312	3.4312	215.551
	G	69	hcp	3.0312	3.0316	4.9497	228.254
			fcc	3.0314	4.2870	4.2870	228.231
			bcc	2.9690	3.4283	3.4283	217.021
	LD	70	hcp	3.0751	3.0756	5.0213	225.703
			fcc	3.0753	4.3492	4.3492	225.728
			bcc	3.0095	3.4751	3.4751	214.452
	AS	68	hcp	3.0244	3.0248	4.9386	230.810
			fcc	3.0247	4.2775	4.2775	230.785
			bcc	2.9620	3.4203	3.4203	219.838
	E	71	hcp	3.1077	3.1081	5.0746	187.902
			fcc	3.1080	4.3953	4.3953	187.863
			bcc	3.0444	3.5153	3.5153	178.553
	LJ	79	hcp	3.0401	3.0404	4.9642	213.647
			fcc	3.0402	4.2996	4.2996	213.632
			bcc	2.9796	3.4406	3.4406	204.381
	RPFS[c]	14	fcc	3.024	4.277	4.277	218.0
Ar	CT[b]	46	hcp	3.7002	3.7006	6.0420	761.596
			fcc	3.7004	5.2332	5.2332	761.508
			bcc	3.6226	4.1830	4.1830	724.711
	LD	70	hcp	3.6820	3.6824	6.0122	718.267
			fcc	3.6822	5.2075	5.2075	718.182
			bcc	3.6036	4.1611	4.1611	686.430
	A	72	hcp	3.6806	3.6810	6.0100	768.847
			fcc	3.6809	5.2055	5.2055	768.753
			bcc	3.6022	7.8602	7.8602	731.862
	SKB	73	hcp	3.6951	3.6954	6.0338	765.033
			fcc	3.6954	5.2260	5.2260	764.942
			bcc	3.6165	4.1760	4.1760	727.567
	MS	74	hcp	3.6789	3.6793	6.0073	786.352
			fcc	3.6791	5.2030	5.2030	786.216
			bcc	3.6293	4.1907	4.1907	744.906
	BP	75	hcp	3.6843	3.6849	6.0160	775.680
			fcc	3.6046	5.2109	5.2109	775.569
			bcc	3.6020	4.1592	4.1592	739.848

TABLE II. (*Continued.*)

Element	Potential	Ref.	Structure	r_{min}^{SS}	$a=b$	c	E_{coh}
	LJ	79	hcp	3.7260	3.7264	6.0843	742.087
			fcc	3.7262	5.2697	5.2697	742.026
			bcc	3.6519	4.2169	4.2169	709.896
	RPFS[c]	14	fcc	3.686	5.213	5.213	760.30
Kr	T[b]	47	hcp	3.9730	3.9735	6.4874	1036.320
			fcc	3.9733	5.6191	5.6191	1036.190
			bcc	3.8890	4.4907	4.4907	985.320
	HC	76	hcp	3.9384	3.9389	6.4310	1092.131
			fcc	3.9387	5.5701	5.5701	1092.004
			bcc	3.8531	4.4491	4.4491	1040.448
	MS	77	hcp	3.9263	3.9264	6.4115	1079.928
			fcc	3.9264	5.5528	5.5528	1079.850
			bcc	3.8413	4.4355	4.4355	1025.268
	AS[d]	78	hcp	3.9276	3.9280	6.4133	1064.662
			fcc	3.9278	5.5548	5.5548	1064.535
			bcc	7.2668	4.4403	4.4403	1013.846
	AS[e]	78	hcp	3.9252	3.9257	6.4095	1080.309
			fcc	3.9255	5.5515	5.5515	1080.179
			bcc	3.8408	4.4350	4.4350	1029.780
	SKB	73	hcp	3.9562	3.9567	6.4600	1041.706
			fcc	3.9565	5.5953	5.5953	1041.564
			bcc	3.8725	4.4715	4.4715	991.078
	LJ	79	hcp	3.9354	3.9357	6.4262	1137.071
			fcc	3.9356	5.5658	5.5658	1136.978
			bcc	3.8571	4.4538	4.4538	1087.761
	RPFS[c]	14	fcc	3.928	5.556	5.556	1062.4
Xe	MS	77	hcp	4.2680	4.2683	6.9693	1515.595
			fcc	4.2681	6.0361	6.0361	1515.469
			bcc	4.1788	4.8253	4.8253	1442.049
	AS	78	hcp	4.2774	4.2780	6.9846	1503.577
			fcc	4.2778	6.0497	6.0497	1503.391
			bcc	4.1865	4.8342	4.8342	1429.096
	SKB	73	hcp	4.3357	4.3362	7.0797	1395.832
			fcc	4.3360	6.1320	6.1320	1395.658
			bcc	4.2432	4.8996	4.8996	1326.864
	LJ	79	hcp	4.4204	4.4208	7.2182	1370.458
			fcc	4.4207	6.2517	6.2517	1370.345
			bcc	4.3325	5.0027	5.0027	1311.021
	RPFS[c]	14	fcc	4.320	6.110	6.110	1492.2

[a]All distances and lattice parameters in Å and cohesive energies in cm^{-1}. For the bcc structure $r_{\min}^{SS}=\sqrt{3/4}a$, and for fcc, $r_{\min}^{SS}=\sqrt{2}a/2$. For the hcp structure $r_{\min}^{SS}=a$ if $c/a=\sqrt{8/3}$. This relation is not exactly fulfilled, and the $r_{\min}^{SS}$ listed differ slightly from the a value. The abbreviation in the Potential column uses the first letters of the authors given in the reference list.

[b]Using Eq. (2) to fit the potential.

[c]The RPFS results of Rosciszewski *et al.* (Ref. 14) are two-body contributions from CCSD(T) results.

[d]HFD-C potential refitted to give Eq. (2).

[e]HFD-B potential.

lattice constants and cohesive energies, and for the fcc structure these agree nicely with the two-body coupled-cluster results of Rosciszewski *et al.*,[22] the exception being the results of Ermakova *et al.*,[71] Leonhard and Deiters,[70] and Tao[47] who used fourth-order many-body perturbation theory (MBPT4) to produce the potential curves. It is obvious that MBPT4 underestimates the cohesive energy by ca. 14% for Ne, 6% for Ar, and 2.5% for Kr. The minimum bond distances of the solid rare gases are all slightly below the distances of the corresponding rare-gas dimer, but well above

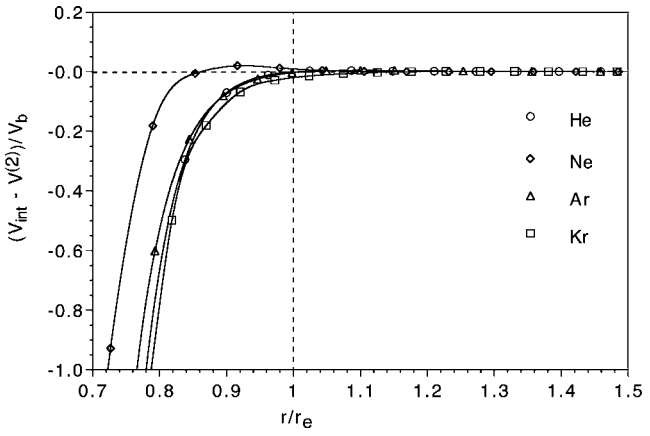

FIG. 4. Sum of three- and higher-order n-body contributions in units of the potential depth V_b as a function of the reduced distance r/r_e. r_e denotes the equilibrium distance.

the hard-sphere radius. This is easily explained by using a simple Lennard-Jones potential as discussed in the following.

For the case of the Lennard-Jones potential, properties like the lattice constants, cohesive energy, and bulk modulus for the Bravais lattices can be derived analytically.[80] We extend this scheme to our more general ansatz (5). If we rewrite Eq. (3) in a form that the distance r is expressed as a dimensionless number $\alpha(\boldsymbol{R})$ depending on the Bravais lattice vector $\boldsymbol{R}$ times the solid-state minimum distance r_{min}^{SS}, we obtain, for the two-body cohesive energy (a minus sign is introduced),

$$E_{coh}^{(2)} = -\frac{1}{2}\sum_{i=1}^{n} L_i c_i (r_{\min}^{SS})^{-i}, \tag{9}$$

where

$$L_i = \sum_{R\neq 0} \alpha(\boldsymbol{R})^{-i} \tag{10}$$

are the Lennard-Jones-Ingham lattice coefficients,[81] which are tabulated by Kane and Goeppert-Mayer for the three cubic Bravais and hcp lattices up to relatively high order in n.[82] In Table VII in the Appendix we list these coefficients to computer accuracy for four different lattices. Equation (9) implies that the cohesive energy can be calculated analytically. For a simple Lennard-Jones (6–12) potential this simplifies to

$$E_{coh}^{(2)} = E_{\min}\left[L_6\left(\frac{r_{\min}}{r^{SS}}\right)^6 - \frac{1}{2}L_{12}\left(\frac{r_{\min}}{r^{SS}}\right)^{12}\right], \tag{11}$$

where E_{min} is the dissociation energy ($E_{min}=-V_{min}$) and r_{min} the equilibrium distance of the gas-phase dimer. From minimization of the potential (11) with respect to the solid-state distance r^{SS} we obtain

$$r_{\min}^{SS} = \left(\frac{L_{12}}{L_6}\right)^{1/6} r_{\min}, \tag{12}$$

where r_{min} is the minimum distance of the two-body potential. This gives the Lennard-Jones ratio of nearest-neighbor distances of $r_{min}/r_{min}^{SS}=(L_6/L_{12})^{1/6}$ between the solid state and the rare-gas dimer in the gas phase. For an fcc lattice we get $r_{min}/r_{min}^{SS}=1.0296$. This ratio is exactly obtained from our solid-state calculations as shown in Table III. Moreover, the ratio r_{min}/r_{min}^{SS} changes only little for all potentials and rare-gas elements applied. From the well-known relation $r_{min}/r_{HS}=2^{1/6}$ we get $r_{HS}<r_{min}^{SS}<r_{min}$. Using Eqs. (11) and (12) we get, for the two-body cohesive energy,

$$E_{coh}^{(2)} = \frac{1}{2}\frac{E_{\min}L_6^2}{L_{12}}. \tag{13}$$

For an fcc lattice we get $E_{coh}^{(2)}/E_{min}=8.6093$. Here all potentials are below the ideal Lennard-Jones value which implies that the Lennard-Jones potential overestimates cohesive energies (if E_{min} corresponds to the exact dissociation energy of the gas-phase dimer). The bulk modulus for the fcc and hcp lattices can also be obtained from Eq. (8),[80]

$$B = L_{12}\left(\frac{2L_6}{L_{12}}\right)^{5/2}\frac{E_{min}}{r_{min}^3}, \tag{14}$$

which gives, for example, $B_{fcc}=3.1283\times 10^7 E_{min}/r_{min}^3$ [kbar], where E_{min} and r_{min} are given in atomic units. For the Lennard-Jones system of He we derive 6.16 kbar, in perfect agreement with our numerical value derived from Eq. (8), Table III.

More accurate two-body cohesive energies, lattice constant, and bulk modulus for the lattices can now be obtained by minimizing Eq. (9) with respect to r^{SS}. The results are given in Table IV and can be compared to the numerical results in Tables II and III, which demonstrates that $N\sim 100\,000$ atoms in our simulations is of sufficient numerical accuracy. Moreover, compared to the results of Stoll and co-workers[14,22] we see that the performance of the more accurate two-body potentials is excellent. We mention that the tiny distortion in the hcp structure resulting in a not ideal c/a ratio of $\sqrt{8/3}$ in the lattice constants leads to an insignificant change in the cohesive energy and can be neglected. We see rather small deviations between the analytical and simulated results for the lattice constants, cohesive energies, and bulk moduli (compare values in Tables II–IV), which, however, do influence the small differences in energy between the hcp and fcc structures (compare the $\Delta E_{hcp/fcc}$ values in Tables III and IV). Hence, for discussing such small energy differences, the extended Lennard-Jones potential (2) becomes quite useful.

The question arises whether or not a physically relevant two-body potential can stabilize the fcc over hcp structure, which was discussed intensively in the 1960s.[2,8] The results in Table II clearly demonstrate that all potentials favor hcp over fcc (if we neglect the ZPVE). Hence it seems that the original suggestion by Kihara and Koba[83] that hcp is favored over fcc for all relevant two-body potentials is correct. For the LJ potential this is easy to prove.[8,24] The difference in the Lennard-Jones-Ingham coefficients for fcc and hcp is shown in Table VII. If we subtract the cohesive energies of both structures according to Eq. (11), we obtain the condition for fcc and hcp being energetically degenerate as a function of the nearest-neighbor distance,[24]

TABLE III. Bulk moduli B (in kbar), minimum solid state distance $r_{\min}^{SS}$ (from Table II), two-body equilibrium bond distance r_{min}, hard-sphere radius r_{HS} (in Å), and ratio between the cohesive energy E_{coh} (Table II) and the two-body dissociation energy E_{min} for the fcc lattice using various two-body potentials. The difference in cohesive energy between the fcc and hcp lattices $\Delta E_{fcc/hcp}=E_{fcc}-E_{hcp}$ is also shown (in cm^{-1}).

Element	Potential	Ref.	B	$r_{\min}^{SS}$	r_{min}	r_{HS}	$r_{min}/r_{\min}^{SS}$	E_{coh}/E_{min}	$\Delta E_{fcc/hcp}$
He	SFR[b]	45	4.61	2.979	3.050	2.702	1.0240	7.540	−0.0076
	PD	66	4.56	2.966	3.032	2.687	1.0222	7.212	−0.0056
	JA	67	5.82	2.896	2.965	2.639	1.0238	7.987	−0.0080
	LJ	79	6.16	2.867	2.952	2.630	1.0296	8.610	−0.0071
Ne	CT[b]	46	19.94	3.034	3.099	2.770	1.0213	7.920	−0.022
	G	69	20.09	3.031	3.096	2.767	1.0213	7.908	−0.022
	LD	70	19.83	3.075	3.140	2.808	1.0210	8.217	−0.015
	AS	68	20.02	3.025	3.091	2.759	1.0219	7.859	−0.025
	E	71	15.44	3.108	3.174	2.838	1.0214	7.897	−0.039
	LJ	79	17.11	3.040	3.130	2.789	1.0296	8.610	−0.015
	RPFS[a]	14 and 22	19.9	3.039	3.105	—	1.022	7.823	−0.029
Ar	CT[b]	46	36.36	3.700	3.778	3.373	1.0210	7.853	−0.088
	LD	70	32.86	3.682	3.768	3.354	1.0234	7.897	−0.085
	A	72	37.02	3.681	3.757	3.350	1.0207	7.722	−0.093
	SKB	73	36.72	3.695	3.771	3.365	1.0206	7.732	−0.091
	MS	74	46.18	3.679	3.761	3.405	1.0223	7.961	−0.136
	BP	75	36.34	3.685	3.757	3.341	1.0195	7.555	−0.121
	LJ	79	32.26	3.726	3.837	3.418	1.0296	8.610	−0.061
	RPFS[a]	14 and 22	37.5	3.686	3.795	—	1.021	7.753	−0.094
Kr	T[b]	47	40.48	3.973	4.051	3.616	1.0194	7.653	−0.130
	HC	76	42.17	3.939	4.023	3.582	1.0214	7.784	−0.128
	MS	74	43.32	3.926	4.007	3.573	1.0204	7.692	−0.078
	AS[b]	78	42.15	3.928	4.011	3.579	1.0213	7.792	−0.127
	AS	78	42.25	3.926	4.008	3.571	1.0210	7.724	−0.130
	SKB	73	40.60	3.957	4.038	3.602	1.0206	7.623	−0.142
	LJ	79	41.95	3.936	4.052	3.610	1.0296	8.610	−0.093
	RPFS[a]	14 and 22	41.7	3.982	4.065	—	1.021	7.730	−0.134
Xe	MS	47	46.51	4.268	4.362	3.890	1.0220	7.751	−0.127
	AS	78	46.80	4.278	4.363	3.892	1.0199	7.663	−0.186
	SKB	73	41.85	4.336	4.421	3.944	1.0195	7.623	−0.174
	LJ	79	35.67	4.421	4.552	4.055	1.0296	8.610	−0.113
	RPFS[a]	14 and 22	46.2	4.320	4.409	—	1.021	7.688	−0.187

[a]The RPFS results of Rosciszewski *et al.* (Ref. 14) are two-body contributions from CCSD(T) results.
[b]Using Eq. (2) to fit the potential.

$$\left[\frac{1}{2}D_{12}\left(\frac{r_{\min}}{r^{SS}}\right)^{12}-D_6\left(\frac{r_{\min}}{r^{SS}}\right)^{6}\right]=0 \quad \text{with } D_n=L_n^{hcp}-L_n^{fcc}, \tag{15}$$

which gives the critical distance r_c^{SS},

$$r_c^{SS}=\left(\frac{D_{12}}{D_6}\right)^{1/6}r_{\min}=\left(\frac{L_6^{fcc}D_{12}}{D_6L_{12}^{fcc}}\right)^{1/6}r_{\min}^{fcc}. \tag{16}$$

This gives $r_c^{SS}=0.8923r_{\min}^{fcc}$. This distance is below the nearest-neighbor distance of the solid. Moreover, for $r^{SS}>r_c^{SS}$ the hcp structure is lower in energy, completing our proof. Koba and Kihara demonstrated that potentials reversing this trend are unphysical.[83]

The cohesive energy difference between the hcp and fcc structures is shown as a function of the nearest-neighbor distance in the solid in Fig. 5, which qualitatively is identical to what is predicted from a LJ potential. The distances where the hcp structure is lowest in energy compared to the fcc structure is 2.691 Å for He, 2.606 Å for Ne, 3.184 Å for Ar, and 3.414 Å for Kr, Fig. 5. For Ne, Ar, and Kr these distances are significantly below the equilibrium solid-state values as expected. It is therefore interesting to ask if at certain pressures a phase transition from fcc to hcp can be achieved. However, even at these small distances we get rather small

TABLE IV. Analytically derived lattice constants a (in Å), cohesive energies E_{coh}, bulk moduli B (in kbar), and differences in energy between the fcc and hcp structures, $\Delta E_{fcc/hcp}=E_{fcc}-E_{hcp}$ (in cm^{-1}), using the two-body potential (2) for three different lattices obtained from Eq. (9). For the lattices we have $a=b$, and for hcp we fixed the ratio $a/c=\sqrt{8/3}$. The references for the potentials are given in Table III.

Element	Potential	Structure	$a=b$	c	E_{coh}	B	$\Delta E_{fcc/hcp}$
He	SFR	hcp	2.9789	4.8645	56.029	4.611	−0.0077
		fcc	4.2128	4.2128	56.021	4.609	
		bcc	3.3652	3.3652	53.736	4.327	
Ne	CT	hcp	3.0338	4.9541	226.746	19.921	−0.0293
		fcc	4.2904	4.2904	226.716	19.918	
		bcc	3.4311	3.4311	215.560	18.361	
Ar	CT	hcp	3.7004	6.0427	761.660	36.343	−0.1031
		fcc	5.2332	5.2332	761.557	36.338	
		bcc	4.1830	4.1830	724.750	33.517	
Kr	T	hcp	3.9732	6.4882	1036.398	40.462	−0.1483
		fcc	5.6190	5.6190	1036.249	40.455	
		bcc	4.4907	4.4907	985.354	37.270	

energy differences for $\Delta E_{fcc/hcp}$ (in cm^{-1}): 0.0098 for He, 0.052 for Ne, 0.185 for Ar, and 0.271 for Kr. These values are below the difference in zero-point vibrational energies between both structures, which favors fcc as we shall see. Moreover, at rather short distances (high pressures) $\Delta E_{fcc/hcp}$ changes sign as expected (Fig. 5); that is, fcc becomes the preferred arrangement. Hence, it is clear that it will be almost impossible to achieve a phase transition from fcc to hcp, and there is no experimental evidence of any phase transition under high pressure except for He and Xe.[84] However, a previous linear muffin-tin orbital study by McMahan suggested a phase transition from fcc to hcp at pressures of <230 GPa.[85] We will discuss this in more detail for Ar since at such high pressures three-body interactions become important. For He, however, the situation is entirely different. Here we have only very small energy differences between fcc and hcp at distances down to 2.39 Å. In the low-pressure range He prefers the hcp structure.[41]

We finally note that the nearest-neighbor distance r_{min}^{SS} in the bcc structure is smaller compared to fcc or hcp; the latter ones show almost equal distances. Hence the ratio in the volume between both structures is much smaller than expected; i.e., for Ar we have $V_{fcc}/V_{bcc}=1.0215$ (the ideal ratio is $\sqrt{32/27}=1.0887$). There is also a small bcc phase which appears in the (P,T) phase diagram of He.[86] It is evident that under higher pressure a phase transition occurs from bcc to the more compact hcp or fcc phase.

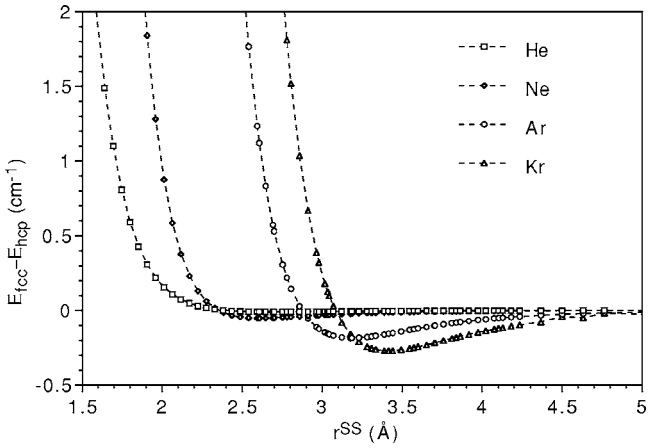

FIG. 5. Difference between fcc and hcp cohesive energies for He, Ne, Ar, and Kr as a function of the nearest-neighbor distance in the solid.

C. Three-body corrections for Ar

It was already pointed out by Lombardi and Jansen[87] that the three-body contributions to the interaction potential are important. In the following, we only consider argon for the discussion of three-body effects. We mention, however, that we also looked at the Ne three-body potential of Ermakova *et al.*[71] However, this potential is attractive in the long-range region and the fcc lattice constant therefore decreases from 4.395 Å to 4.365 Å in contradiction of the more accurate solid-state results of Rosciszewski *et al.*,[14] where the lattice constant increases by 0.019 Å. In Table VI below, we have the optimized lattice constants for both the fcc and hcp structures. Our results clearly support the conclusion of Rosciszewski *et al.*[14] that three-body effects will not stabilize the fcc over the hcp structure.

The solid-state interaction curve including the three-body potential is shown in Fig. 6, and the corresponding density-pressure relationship is shown in Fig. 7. Here the pressure is obtained numerically using as a change of the internal energy with respect to the volume of the unit cell. At low pressure both curves obtained from two- and two-plus-three body interactions are very close to the experimental curve.[64] The small but systematic error in this low-pressure region comes from the density at zero temperature and pressure. From experiment we have 1.7710 ± 0.0001 g/cm^3. Our two-body potential at the minimum distance gives 1.8514 g/cm^3. Taking three-body effects into account we get 1.8123 g/cm^3, in much better agreement with experiment. The remaining error is due to inaccuracies in the two- and three body potentials, the neglect of higher than three-body interactions, and zero-

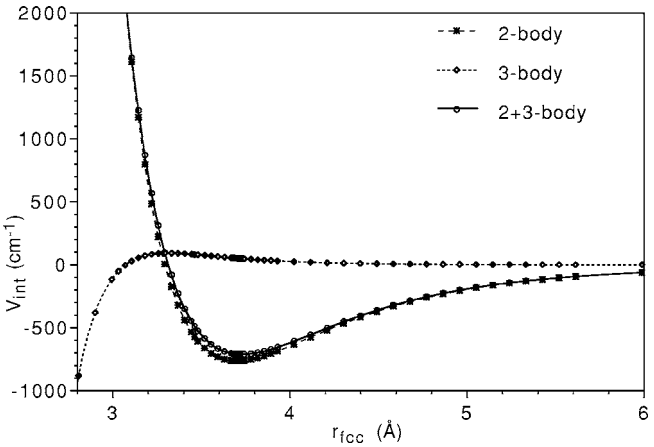

FIG. 6. Two- and three-body contributions for the interaction potential of solid Ar.

point vibrational effects. If we correct for these by shifting the curve to the experimental density, we get almost perfect agreement with experiment.

More interesting is the high-pressure region.[88] Under high pressure (small distances) three- and higher-body terms become more important as discussed above. It is perhaps useful to give a rough estimate when such interactions cannot be neglected anymore. For the Lennard-Jones solid we can estimate when the repulsive region starts by using $E_{coh}=0$ in Eq. (11). This gives the solid-state hard-sphere radius

$$r_{HS}^{SS}=\left(\frac{L_{12}}{2L_6}\right)^{1/6} r_{\min}, \tag{17}$$

and not surprisingly, there is only a factor of $2^{1/6}$ difference between r_{HS}^{SS} and $r_{\min}^{SS}$. This gives $r_{HS}^{SS}=0.8653 r_{\min}$, and according to Fig. 3 three-body contributions from Ne to Kr contribute to roughly 10% to the total energy. If we take this as the onset of the importance of three-body interactions, we can estimate the pressure required to reduce the nearest-neighbor solid-state distance to r_{HS}^{SS},

$$P=-\frac{\partial V_{\text{int}}}{\partial v}\approx\frac{2^{1/2}E_{coh}}{(r_{HS}^{SS})^3}=\frac{E_{\min}L_6^{5/2}}{L_{12}^{3/2}(r_{\min})^3}=2^{5/2}B_{fcc}, \tag{18}$$

where v is the volume per particle for a fcc lattice. This gives about 6 GPa for Ne, 15 GPa for Ar, and 20 GPa for both Kr and Xe using experimental values for the bulk moduli.[89–92] Figure 7(a) nicely shows that three-body effects start to become important at around 15 GPa, the point where the two-body curve starts to deviate from the experimental values. Even more interestingly, we see deviations between the two-plus-three body curve and the experimental line at 30 GPa, the region where higher than three-body effects start to become important. However, in this region all known two-body curves deviate substantially, often by a factor of 2. Our potential was fitted to distances down to about 3 Å, giving accurate values only up to 30 GPa. The Aziz two-body potential which gets the repulsive wall from Hartree-Fock and experimental data is also shown in Fig. 7(a). This potential lies slightly above the experimental curve, but follows the line closely up to 100 GPa. The Lennard-Jones curve is

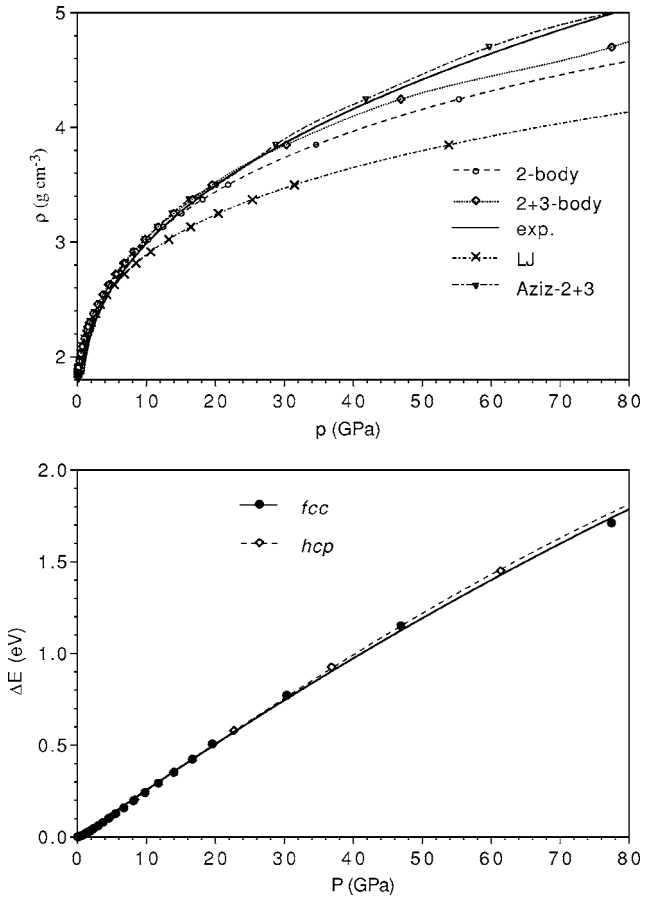

FIG. 7. (a) Top: Density of solid argon versus pressure for two- and two-plus-three-body interaction potentials. Experimental curve from Ref. 64. (b) Bottom: Energy change for solid argon with increasing pressure.

clearly not designed for the repulsive region as Fig. 7(a) shows. Figure 7(b) also shows the difference in energy between fcc and hcp up to 80 GPa including three-body effects. At higher pressures the hcp energy curve is always above the fcc curve as found for the two-body case (Fig. 5); thus, up to this pressure range there seems to be no phase transition taking place. Of course, this analysis neglects vibrational and higher than three-body effects. We argue that more accurate two-body potentials for the short range are needed to discuss the high-pressure range.

D. Clusters

The rather tiny energy differences between the fcc and hcp structures do not explain why experimentally only the fcc structure is observed for Ne and all other heavier rare-gas elements, even though inclusion of the zero-point vibrational energy finally brings the solid to the fcc structure. We therefore looked at growth patterns of rare-gas clusters. Figure 8 shows a comparison of dissociation energies (per atom) for the global minimum cluster structures ("icosahedral" growth pattern) as well as fcc and hcp structures using our two-body potentials as shown in Eq. (2) with the parameters in Table I. Here we take the exact two-body summation for finite sys-

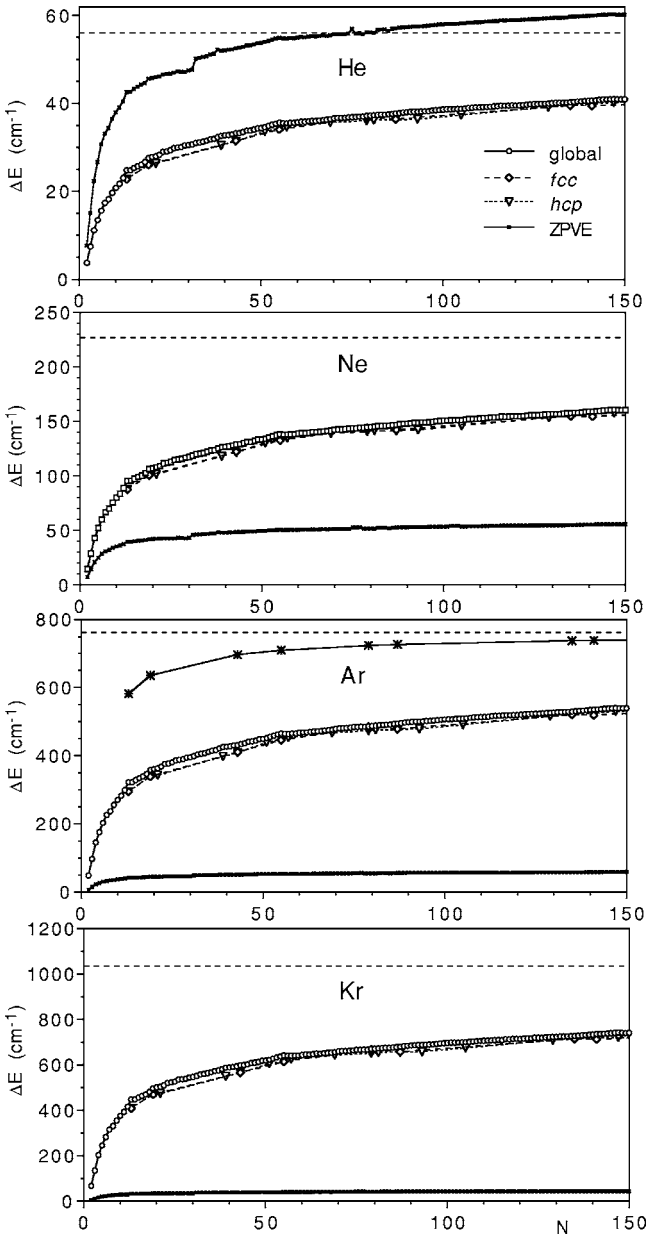

FIG. 8. Cluster dissociation energies per atom as a function of the number of atoms N. For comparison the corresponding optimized clusters kept in fcc and hcp solid-state symmetry and zero-point vibrational energies are also shown. The corresponding calculated cohesive energy is shown as a dashed line at the top of the graph. For Ar we include the energies obtained from Eq. (5) which does not include surface effects and converges much faster towards the exact two-body cohesive energy (curve closest to the cohesive energy line).

FIG. 9. The (a) fcc, (b) hcp, and (c) global minimum LJ-type structures of Ar_{79} for comparison.

tems including the high-energy surface effects. To keep these surface effects as small as possible, however, the cluster growth for the hcp and fcc structures is in form of shells with equal nearest-neighbor distances, such that the overall structure is relatively compact and almost spherical, and close to the Lennard-Jones type global minimum structures; see Fig. 9.

The per-atom dissociation energies of the optimized rare-gas clusters all follow similar qualitative trends, Fig. 8. There is a rapidly increasing stabilization range for the smallest cluster sizes followed by a very slow but monotonous trend towards the asymptotic cohesive energy. For argon we show for comparison the energies calculated from Eq. (5) which gives a much faster convergence towards the solid state as surface effects are not included, Fig. 8. We mention that at a size of 5000 particles we obtain a much reduced $E_{coh}=685.0\ \mathrm{cm}^{-1}$ and $B=32.7$ kbar for the fcc lattice of Ar using Eq. (1) for the two-body potential. This demonstrates that surface effects are still large at this size.

The atomic binding energies $\Delta E(N)=E(N)-E(N-1)$ also follow a trend which is qualitatively similar for all the rare

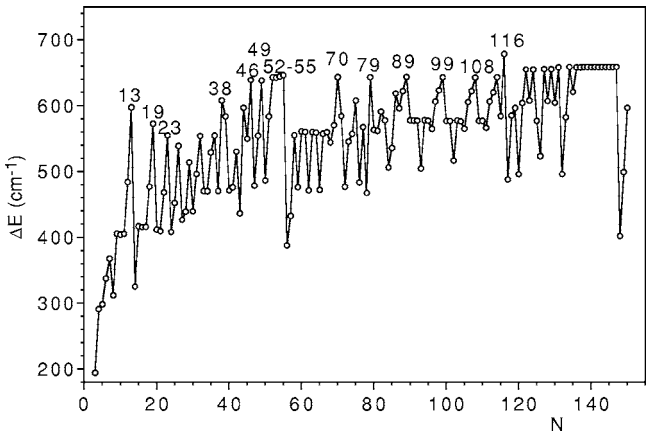

FIG. 10. Atomic binding energies $\Delta E(N)=E(N)-E(N-1)$ for Ar as a function of the cluster size N.

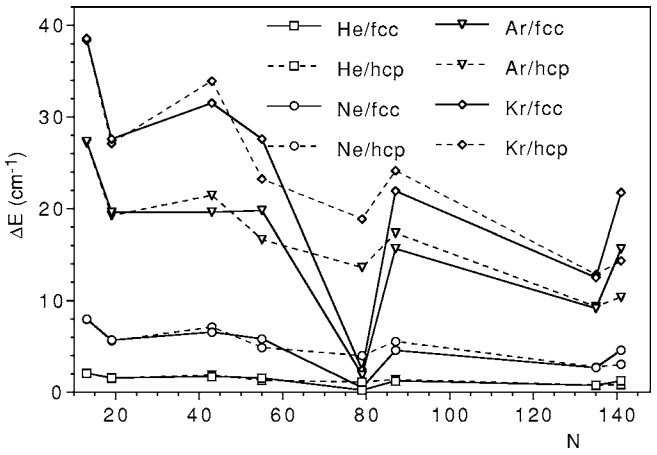

FIG. 11. Difference between the global minimum structures and fcc and hcp structures for He, Ne, Ar, and Kr as a function of the cluster size.

gases, but show some deviations from the corresponding trend for the LJ clusters as can be seen in Fig. 10 for Ar. For instance, there are few differences in some of the magic numbers predicted using the LJ potential and the LJ-modified potentials for this work; at sizes like 116, we find a minimum (particularly pronounced for the cases of argon and krypton) that does not occur for the LJ clusters, while at $N=135$ we do not find the magic structure that is so conspicuous for LJ clusters. The trends of the $\Delta E(N)$ are also slightly different in the qualitative behavior in a few other N ranges. When comparing the $\Delta E(N)$ trend for our argon clusters with that from the calculations by Naumkin and Wales[93] performed for the same clusters but using the Aziz potential,[72] we see a complete correspondence of the trends for all cluster sizes for which data are available ($N\leqslant 55$).

On the energy scale shown in Fig. 8 the fcc and hcp per-atom dissociation energies are very close to the energies of the global minimum structures. Figure 11 clearly shows that the differences between the global minima (GM) clusters and the fcc or hcp structures are quite small with increasing cluster size. In fact, in this range ($N\leqslant 150$) the smallest energy difference is obtained for R_{79}; for example, for Ar_{79} we have $E_{fcc}-E_{GM}=1.9$ cm^{-1}, whereas for hcp the smallest value in this range is obtained for Ar_{135} and for Ar_{147} with $E_{hcp}-E_{GM}=9.4$ and 10.4 cm^{-1}, respectively. These values will get smaller for larger cluster sizes to a point where we have possible transitions to the fcc solid-state structure. To simulate this transition is a challenge for future work. Figure 12 shows fcc versus hcp for clusters up to 5000 atoms. At this large cluster size the convergence towards the more stable hcp structure (neglecting zero-point vibrational and higher many-body effects) is not evident. There are cluster size regions where the fcc structure is the most stable one. This is clearly a surface effect, but also demonstrates that at a certain cluster size the transition to the fcc structure is energetically preferred.

We mention that the largest distance from an atom to the center of mass increases with N in steps, which is related to building a shell structure of the cluster. The formation of a new step for the maximal distance occurs at the next higher cluster size after the occurrence of a magic number in most of the cases. On the other hand, the minimal radius (nearest-neighbor distance) follows a complex trend with no clear relationship to the shell formation.

From plotting the dissociation energy per atom against $N^{-1/3}$ we obtain from an extrapolation to $N\rightarrow\infty$, the cohesive energies of 55.2 cm^{-1}, for He, 219 cm^{-1} for Ne, 735 cm^{-1} for Ar, and 1003 cm^{-1} for Kr, Fig. 13. This is in rather good agreement with the exact two-body energies shown in Table IV, which demonstrates that the $N^{-1/3}$ law is rather well fulfilled for cohesive energies.

E. Zero-point vibrational energy from the bulk

Considering the harmonic ZPVE's, the classical cluster description could be considered a good approximation for the argon and krypton clusters, but less appropriate in the case of neon for which the ratio of the ZPVE to the binding energy goes from 1/2 to about 1/3 when N increases towards the bulk. This behavior agrees with the results of the studies already mentioned about the quantum delocalization in rare-gas clusters. The cluster and solid-state calculations of helium clusters performed for the sake of comparison[94] also support this view, as the harmonic ZPVE's were found

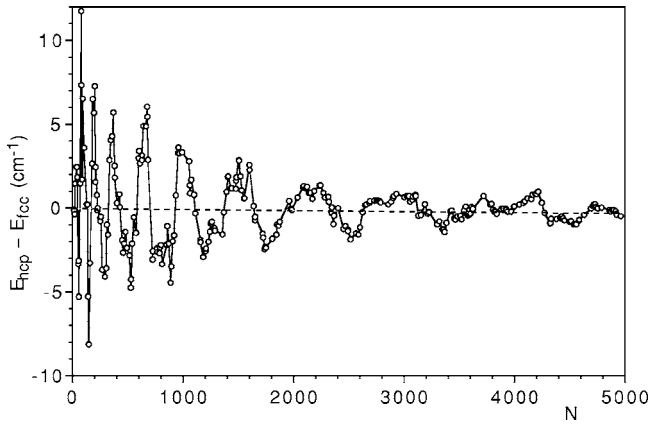

FIG. 12. Difference between fcc versus hcp interaction energies as a function of cluster size N.

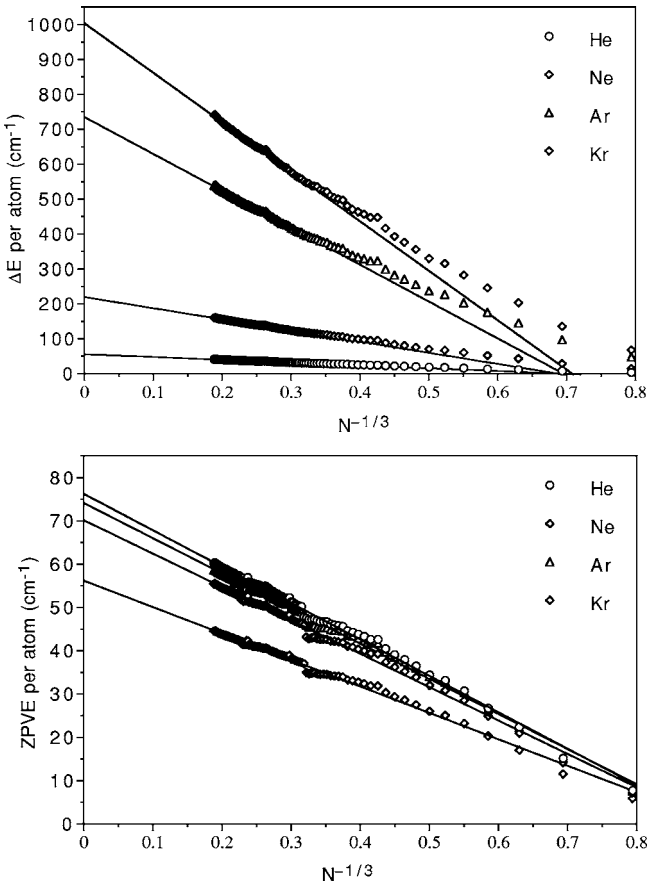

FIG. 13. The cohesive energy and zero-point vibrational energy as a function of $N^{-1/3}$. The linear fit $\Delta E = aN^{-1/3} + b$ shows the extrapolation towards $N \rightarrow \infty$. For details see text.

to be above the corresponding dissociation energies regardless of the cluster size and up to the bulk. Here anharmonicity effects lead to an *increase* of the ZPVE by as much as 23%, Table V. Hence at the optimized two-body lattice constant solid He remains on the repulsive part of the potential energy surface, and a geometry optimization including both harmonic and anharmonic vibrational effects leads to a large expansion of the bulk up to a point where the diagonal force constants become zero (at 4.9 Å). At this point the perturbative treatment of anharmonicity effects completely fails and the position of the He atom in the fixed bulk lattice environment becomes unstable; that is, the system breaks symmetry. These results are consistent with the findings of Glyde.[41] This explains why high pressure is needed to solidify He. For Ne the situation changes and stable lattice parameters are obtained. For example, using the Cybulski-Toczylowski two-body potential[46] we obtain a change in the fcc lattice constant of $\Delta a = 0.179$ Å, due to harmonic ZPVE contributions within the Einstein approximation, and $\Delta a = -0.012$ Å from additional anharmonicity effects. Although all calculated ZPVE values are to be corrected by more precise anharmonicity and additional nonadditive terms, the predicted magnitudes of the delocalization effects decrease with atomic number and cluster size in accordance with the outcomes of previous studies. We mention that He_2 is well known to just accommodate one vibrational level.[95] Therefore anharmonic corrections together with other well-known contributions (relativistic effects, non-Born-Oppenheimer effects, etc.) are crucial for the correct description of these systems.

Table V compares both frequencies obtained from the simple Einstein approximation and the more accurate coupled harmonic treatment taking the full two-body force

TABLE V. Zero-point vibrational energy (in cm^{-1}) calculated by using the Einstein model from moving the central atom in the field of all other fixed atoms (*E*). Anharmonic value from a numerical solution of the vibrational Schrödinger equation for case (*E*). Fully coupled harmonic solution from a harmonic frequency analysis (*C*). The cluster values are obtained from an extrapolation as shown in Fig. 14. $\Delta E_{fcc/ss}$denotes the energy difference between the fcc and the other solid state structures (hcp or bcc). ω_{max} is the maximum phonon frequency. Debye frequencies are from Refs. 2 and 80. For helium the isotope is chosen; otherwise, standard mean atomic masses are used. The frequencies are calculated at the crystal structures obtained from two-body forces as shown in Table IV.

Atom		*E*-harm.	*E*-anharm.	*C*-harm.	Debye	Ref. 14	$\Delta E_{fcc/ss}$	ω_{max}
He	hcp	77.35	17.9	74.27			0.79	74.50
	fcc	77.34	17.9	73.48				74.62
	bcc	76.65	17.8	70.75	26.5		−2.73	74.77
	cluster			76.2				
Ne	hcp	71.76	3.90	68.98			0.69	68.82
	fcc	71.76	3.90	68.29	52.1	46.7		68.90
	bcc	70.72	3.85	65.15			−3.14	69.02
	cluster			70.1				
Ar	hcp	76.10	1.22	73.15			0.74	72.98
	fcc	76.09	1.22	72.41	72.7	63.3		73.09
	bcc	74.97	1.19	69.08			−3.33	73.15
	cluster			74.1				
Kr	hcp	57.38	0.55	55.17			0.50	54.99
	fcc	57.38	0.48	54.62	56.0	47.1		55.09
	bcc	56.49	0.47	52.04			−2.69	55.12
	cluster			56.2				

field into account. The Einstein approximation leads to ZPVE's ($E_{ZPVE}=3\omega_E/2$ where ω_E is the Einstein frequency) which are overestimated by 2–4 cm^{-1} as one expects.[96] Interestingly, the extrapolated ZPVE's from cluster calculations are in very good agreement with our more accurate solid-state results. We also list the maximum phonon frequency ω_{max} and anharmonicity effects in Table V. As one expects, anharmonicity effects become smaller with increasing mass of the rare-gas atoms, and already for argon such effects become relatively small and may therefore be neglected. Moreover, anharmonicity effects will not contribute significantly towards the energy difference between the fcc and hcp structures, in agreement with the results obtained for Ar by Lotrich and Szalewicz.[12] We mention that for better comparison with our cluster results, the values in Table V are obtained at the lattice structures optimized by using two-body potentials only. The ZPVE corrections are therefore larger compared to the results of Rosciszewski *et al.*[14] Nevertheless, our results show that for all rare gases the coupling between the harmonic modes is responsible for fcc being more stable than hcp, as the Einstein approximation leads to insignificant energy differences. Hence, one cannot simply multiply the Einstein frequencies by the factor of $C=\sqrt{15/16}$ derived from Domb and Salter[96] to obtain reliable energy differences for the ZPVE between fcc and hcp, which explains the small differences in ZPVE's obtained by Lotrich and Szalewicz.[12] Our analysis, of course, neglects three-body effects for the cohesive energy, which we analyze for argon in more detail. The question also arises if $N_{vib}=5000$ atoms for the vibrational analysis is sufficiently large. Figure 14 shows a relatively slow convergence of the ZPVE with the dimension of the force field matrix chosen for Ar. An $N^{-1/3}$ extrapolation[97] leads to a ZPVE contribution of 63.5 cm^{-1}, in excellent agreement with Rosciszewski *et al.* (63.3 cm^{-1}).[14] This compares to 63.8 cm^{-1} for $N_{vib}=5000$. In comparison, the Debye frequency 72.7 cm^{-1} (Table V) is overestimated.[2] Another interesting result from the coupled-harmonic calculations is that we have $\omega_E \approx 2\omega_{max}/3$ for all rare-gas elements.

For argon accurate experimental values for the fcc lattice constant a (5.311 Å), cohesive energy E_{coh} (646.1 cm^{-1}), bulk modulus B (26.7 kbar), and maximum phonon energy (67.1 ± 0.05 cm^{-1} at 10 K) (Ref. 98) are available. These compare well with our results for the (2+3+C) case as shown in Table VI—i.e., $a=5.331$ Å, $E_{coh}=645.0$ cm^{-1}, $B=27.7$ kbar, and $\omega_{max}=61.8$ cm^{-1}—and are also close to the theoretical results of Rosciszewski *et al.*[14] We also mention that the anharmonicity effects obtained for argon by Lotrich and Szalewicz[12] at the experimental lattice constant (1.0 cm^{-1}) are comparable to our value (1.2 cm^{-1}). Taking this into account we obtain a cohesive energy of 643.8 cm^{-1}, 2.3 cm^{-1} below the experimental value. Most of this deviation originates from the two-body potential we used which gives a potential depth of 97.0 cm^{-1} (Table I) compared to the estimated value of 99.6 cm^{-1}.[68,72,99]

The extrapolated cluster zero-point vibrational energies are a few cm^{-1} above the coupled phonon solid-state treatment. This could suggest that vibrational effects cannot be neglected in the discussion of a phase change from icosahedral to fcc with increasing cluster size, but this has to be investigated in more detail.

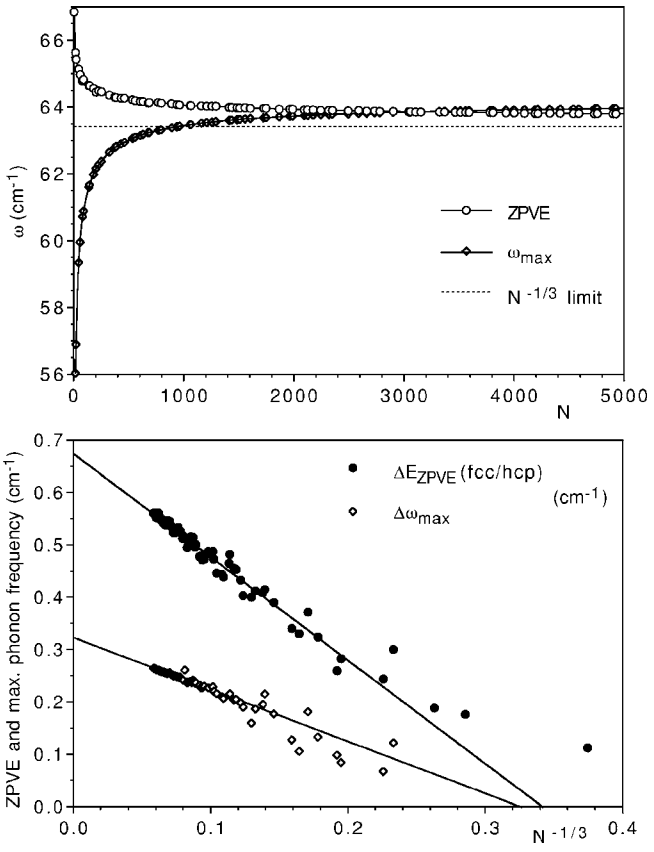

FIG. 14. The zero-point vibrational energy (ZPVE) and maximum phonon frequency ω_{max} for fcc argon in the harmonic approximation as a function of cluster size N. The N atoms used for the vibrational analysis are embedded in a cluster of ca. 130 000 atoms kept in fcc symmetry. The dashed line shows the linear fit $\Delta\omega=aN^{-1/3}+b$ with extrapolation towards $N\rightarrow\infty$ for the ZPVE. Calculations are done at the experimental structure (see Table VI).

Finally, we can address the problem of the fcc versus hcp packing for realistic two-body potentials. A $N^{-1/3}$ extrapolation for the fcc and hcp lattices at the experimental lattice parameters (using the same minimal distances for hcp compared to fcc) gives a difference of 0.67 cm^{-1} for the ZPVE and 0.35 cm^{-1} for ω_{max}. Hence, the results by Rosciszewski *et al.* are now confirmed,[14] and the original argument by Jansen that three-body effects are responsible for the phase change[26] is incorrect. A (2+3)-body optimization (Table VI) for argon including the ZPVE from the Einstein approximation does not lead to a preference for the fcc structure. We note that the lattice parameters are significantly influenced by ZPVE effects even for a heavy element like argon, while anharmonicity effects only lead to minor changes. In any case, the Einstein approximation leads to lattice parameters which are only slightly overestimated. As vibrational effects become less important with the increasing mass of the atom, the energy difference between fcc and hcp becomes smaller as well; see Table V.

TABLE VI. fcc and hcp lattice constants a (in Å), cohesive energies E_{coh} (in cm^{-1}) bulk moduli B (in kbar), and differences in energy, $\Delta E_{fcc/hcp}=E_{fcc}-E_{hcp}$ (in cm^{-1}), for Ar, using the analytical form of the Cybulski-Toczylowski two-body potential and the Lotrich-Szalewicz three-body contributions from a simulation of 50 000 atoms. $2+E$ denotes the use of a two-body potential including the harmonic zero-point vibrational energy (ZPVE) correction applying the Einstein approximation. A denotes that anharmonicity effects are included. $2+3+C$ denotes two- and three-body potentials including the harmonic ZPVE from a simulation of moving 5000 atoms in the field of over 200 000 atoms.

Struct.	Method	$a=b$	c	E_{coh}	B[a]	$\Delta E_{fcc/hcp}$
hcp	2	3.7006	6.0419	761.635	36.3	
	$2+E$	3.7433	6.1115	689.136	28.5	
	$2+AE$	3.7427	6.1107	687.857	28.6	
	$2+C$	3.7408	6.1086	691.763	30.8	
	2+3	3.7273	6.0867	709.914	34.8	
	$2+3+E$[b]	3.7724	6.1603	642.093	28.0	
	$2+3+C$[b]	3.7702	6.1567	644.463	27.6	
fcc	2	5.2332	5.2332	761.534	36.3	−0.101
	$2+E$	5.2936	5.2936	689.040	28.5	−0.096
	$2+AE$	5.2929	5.2929	687.761	28.5	−0.096
	$2+C$	5.2798	5.2798	692.272	30.9	+0.509
	2+3	5.2712	5.2712	709.903	34.8	−0.011
	$2+3+E$	5.3350	5.3350	642.072	27.8	−0.021
	$2+3+C$	5.3305	5.3305	644.964	27.7	+0.501
	2+3[c]	5.249	5.249	714.7	33.6	−0.070
	$2+3+C$[c]	5.311	5.311	645.9	27.9	+0.62
	Expt.[d]	5.311	5.311	646.1	26.7	

[a]The last digit of the bulk modulus may vary with the degree of the polynomial applied in the numerical fit procedure, that is the numerical accuracy of the three-body interaction and the phonon branches are not accurate enough to the third digit. Both contributions show very large gradients with a very small curvature with respect to the lattice constants.

[b]$a/c=\sqrt{8/3}$ is used.

[c]Results from Rosciszewski *et al.* (Ref. 14).

[d]Experimental values from Refs. 100 and 101.

IV. CONCLUSION

Much work has still to be done for constructing accurate two- and three-body interaction potentials for the rare gases. Solid-state calculations will be of great use in the future determination of the accuracy of such potentials, which can be further used in cluster simulations. It is also clear that more work is needed in correctly describing the repulsive region from first-principles quantum theoretical methods. Moreover, for the heaviest rare-gas systems Kr and beyond currently available two-body potentials are not very accurate, often missing important effects like spin-orbit coupling. We demonstrated that the extended Lennard-Jones ansatz is very useful for obtaining analytic values for solid-state properties. The rare-gas problem has now been solved for the many-body expansion, and the previous conclusions drawn by Barron and Domb,[24] and more recently by Rosciszewski *et al.*,[14] can be confirmed. For Xe we expect much lower zero-point vibrational energy contributions and it is therefore of no surprise that an intermediate pressure range is found for a fcc to hcp phase transition.[84] To correctly describe the phase diagrams by theoretical methods for such systems remains a challenge in computational physics.

ACKNOWLEDGMENTS

This work was supported by the Marsden Fund administered by the Royal Society of New Zealand and the Alexander von Humboldt Foundation (Bonn). We are grateful to the Allan Wilson Centre for large amounts of computer time on their high-performance parallel computer HELIX. P.S. is grateful to Tilo Söhnel, Matthias Lein, and Gaven Martin for useful discussions and to Krzystof Szalewicz for making his three-body potential program of argon available to us. We are also grateful to Christian Thierfelder for useful discussions concerning the Lennard-Jones-Ingham coefficients.

APPENDIX

The Lennard-Jones-Ingham lattice coefficients L_m are listed in Table VII from $m=4$ to $m=30$ (note that $L_m=\infty$ for $m\leqslant 3$) to computer accuracy for the simple cubic (sc), body-centered-cubic (bcc), face-centered-cubic (fcc), and hexagonal closed-packed (hcp) lattices. The following

TABLE VII. The dimensionless Lennard-Jones-Ingham lattice coefficients L_m from $m=4$ to $m=30$ for the simple cubic (sc), body-centered-cubic (bcc), face-centered-cubic (fcc), and hexagonal-closed-packed (hcp) lattices.

	sc	bcc	fcc	hcp	$L^{hcp}-L^{fcc}$
L_4	1.6531489(+1)	2.2637791(+1)	2.5337110(+1)	2.5337926(+1)	8.1160(−4)
L_5	1.037752479070(+1)	1.475850933310(+1)	1.696751839999(+1)	1.696843628985(+1)	9.17889865(−4)
L_6	8.40192397482537(+0)	1.22536678672899(+1)	1.44539210437416(+1)	1.44548972778391(+1)	9.76234097517903(−4)
L_7	7.46705778091867(+0)	1.10542434792442(+1)	1.33593877007417(+1)	1.33603467761953(+1)	9.59075453534908(−4)
L_8	6.94580792722634(+0)	1.03551979084025(+1)	1.28019372313780(+1)	1.28028218528098(+1)	8.84621431787025(−4)
L_9	6.62885919888677(+0)	9.89458965632110(+0)	1.24925467021375(+1)	1.24933217250017(+1)	7.75022864223374(−4)
L_{10}	6.42611910253308(+0)	9.56440061535995(+0)	1.23112456654774(+1)	1.23118962338190(+1)	6.50568341587388(−4)
L_{11}	6.29229449923457(+0)	9.31326253739910(+0)	1.22009203512771(+1)	1.22014470998319(+1)	5.26748554824152(−4)
L_{12}	6.20214904504752(+0)	9.11418326807536(+0)	1.21318801965446(+1)	1.21322937690989(+1)	4.13572554348818(−4)
L_{13}	6.14059958002169(+0)	8.95180731857472(+0)	1.20877263213521(+1)	1.20880425502984(+1)	3.16228946392272(−4)
L_{14}	6.09818412571215(+0)	8.81677022848592(+0)	1.20589919443509(+1)	1.20592282550682(+1)	2.36310717385280(−4)
L_{15}	6.06876429503889(+0)	8.70298455998093(+0)	1.20400240550991(+1)	1.20401971443472(+1)	1.73089248132641(−4)
L_{16}	6.04826346958584(+0)	8.60625404754453(+0)	1.20273548440186(+1)	1.20274794193038(+1)	1.24575285282091(−4)
L_{17}	6.03392931636721(+0)	8.52353125043930(+0)	1.20188094367105(+1)	1.20188977196229(+1)	8.82829124062567(−5)
L_{18}	6.02388170786671(+0)	8.45250316860838(+0)	1.20129983096660(+1)	1.20130600231774(+1)	6.17135114513445(−5)
L_{19}	6.01682545633174(+0)	8.39135079141312(+0)	1.20090196044393(+1)	1.20090622241112(+1)	4.26196718859018(−5)
L_{20}	6.01186283088995(+0)	8.33860400567956(+0)	1.20062800413263(+1)	1.20063091581147(+1)	2.91167883172960(−5)
L_{21}	6.00836875754668(+0)	8.29305037041529(+0)	1.20043848093623(+1)	1.20044045100848(+1)	1.97007224667089(−5)
L_{22}	6.00590652613429(+0)	8.25367521808478(+0)	1.20030685693229(+1)	1.20030817842333(+1)	1.32149103748702(−5)
L_{23}	6.00417024007075(+0)	8.21962053488365(+0)	1.20021514909747(+1)	1.20021602867393(+1)	8.79576460555143(−6)
L_{24}	6.00294520818413(+0)	8.19015547548316(+0)	1.20015108249397(+1)	1.20015166385770(+1)	5.81363733509477(−6)
L_{25}	6.00208052037491(+0)	8.16465435192733(+0)	1.20010622787093(+1)	1.20010660971420(+1)	3.81843278418614(−6)
L_{26}	6.00146997249609(+0)	8.14257961592080(+0)	1.20007476748977(+1)	1.20007501686245(+1)	2.49372675575898(−6)
L_{27}	6.00103875223831(+0)	8.12346831587279(+0)	1.20005266902122(+1)	1.20005283104285(+1)	1.62021633975939(−6)
L_{28}	6.00073412107079(+0)	8.10692107103872(+0)	1.20003712775531(+1)	1.20003723253224(+1)	1.04776932907669(−6)
L_{29}	6.00051887921221(+0)	8.09259293837612(+0)	1.20002618714474(+1)	1.20002625461501(+1)	6.74702711478403(−7)
L_{30}	6.00036677489718(+0)	8.08018574990617(+0)	1.20001847900598(+1)	1.20001852228518(+1)	4.32791969373625(−7)
L_∞	6	8	12	12	0

formulas were used, which are often incorrectly given in the literature:[2]

$$L_m^{sc} = \sum_{i,j,k \in Z\backslash(0,0,0)} (i^2 + j^2 + k^2)^{-m/2}, \tag{A1}$$

$$L_m^{bcc} = \left(\frac{\sqrt{3}}{2}\right)^m \left\{ L_m^{sc} + \sum_{i,j,k \in Z} \left[\left(i + \frac{1}{2}\right)^2 + \left(j + \frac{1}{2}\right)^2 + \left(k + \frac{1}{2}\right)^2 \right]^{-m/2} \right\}, \tag{A2}$$

$$L_m^{fcc} = 3 \sum_{i,j,k \in Z\backslash(0,0,0)} (2i^2 + j^2 + k^2)^{-m/2} - 2^{1-m/2} L_m^{sc}, \tag{A3}$$

$$L_m^{hcp} = \sum_{i,j,k \in Z\backslash(0,0,0)} \left(i^2 + j^2 + ij + \frac{8}{3}k^2\right)^{-m/2} + \sum_{i,j,k \in Z} \left[\left(i + \frac{1}{3}\right)^2 + \left(j + \frac{1}{3}\right)^2 + \left(i + \frac{1}{3}\right)\left(j + \frac{1}{3}\right) + \frac{8}{3}\left(k + \frac{1}{2}\right)^2 \right]^{-m/2}. \tag{A4}$$

Here Z denotes all positive and negative integers and $Z\backslash(0,0,0)$ denotes that the case $i=j=k=0$ is excluded. The formulas may be further simplified taking into account the symmetry of positive and negative integers. $m=4$ is a special case, and the sums for the cubic cases can be rewritten in a more practical form using generalized ζ functions.[48] For the $m \leqslant 3$ the series L_m^{sc} is, however, divergent.[81] We present a more straightforward proof. It is sufficient to show that the first series in L_m^{sc} is divergent. Using the Cauchy integral criterion it is sufficient to show that the following integral is divergent:

$$\int\int\int_{[1,\infty)} (x^2+y^2+z^2)^{-m/2} d\mathbf{r} = 4\pi \int_{[\sqrt{3},\infty)} r^{-m+2} dr. \tag{A5}$$

It is clear that the integral diverges for $m \leqslant 3$. Hence, the Lennard-Jones-Ingham lattice coefficients are listed only from $m=4$ onwards as indeed pointed out by Lennard-Jones in 1924.[48] We also note the work of Zucker[102] on Madelung constants for invariant cubic lattice complexes. A comparison to his coefficients shows that for the smaller m values our L_m^{sc} coefficients are not converged out to the accuracy given in the Table, especially for $m \leqslant 8$. This will be addressed in a subsequent paper.

*Electronic address: p.a.schwerdtfeger@massey.ac.nz

[1] S. Rick, D. L. Lynch, and J. D. Doll, J. Chem. Phys. **95**, 3506 (1991).
[2] M. L. Klein and J. A. Venables, *Rare Gas Solids* (Academic Press, London, 1976), Vol. 1.
[3] D. J. Wales and J. P. K. Doye, J. Phys. Chem. A **101**, 5111 (1997).
[4] J. P. K. Doye, D. J. Wales, and M. A. Miller, J. Chem. Phys. **109**, 8143 (1998).
[5] J. P. K. Doye, M. Miller, and D. J. Wales, J. Chem. Phys. **111**, 8417 (1999).
[6] V. Kumar, Prog. Cryst. Growth Charact. Mater. **34**, 95 (1997).
[7] B. Hartke, Angew. Chem., Int. Ed. **41**, 1468 (2002).
[8] M. Born, Proc. Cambridge Philos. Soc. **36**, 160, (1940); **36**, 173 (1940); **38**, 62 (1942); **38**, 82 (1942); **40**, 262 (1944);
[9] J. A. Prins, J. M. Dumore, and L. T. Tjoan, Physica (Amsterdam) **18**, 307 (1952).
[10] T. Kihara and S. Koba, J. Phys. Soc. Jpn. **7**, 348 (1952).
[11] G. L. Pollack, Rev. Mod. Phys. **36**, 748 (1964).
[12] V. F. Lotrich and K. Szalewicz, Phys. Rev. Lett. **79**, 1301 (1997).
[13] L. Jansen, Phys. Rev. **135**, A1292 (1964).
[14] K. Rosciszewski, B. Paulus, P. Fulde, and H. Stoll, Phys. Rev. B **62**, 5482 (2000).
[15] W. Kohn, Y. Meir, and D. E. Makarov, Phys. Rev. Lett. **80**, 4153 (1998).
[16] J. Tao and J. Perdew, J. Chem. Phys. **122**, 114102 (2005).
[17] T. Sato, T. Tsuneda, and K. Hirao, Mol. Phys. **103**, 1151 (2005).
[18] E. Goll, H.-J. Werner, and H. Stoll, Phys. Chem. Chem. Phys. **7**, 1 (2005).
[19] M. Dion, H. Rydberg, E. Schröder, D. C. Langreth, and B. I. Lundqvist, Phys. Rev. Lett. **92**, 246401 (2004).
[20] D. M. Deaven, N. Tit, J. R. Morris, and K. M. Ho, Chem. Phys. Lett. **256**, 195 (1996).
[21] V. Schwarz, H. Juranek, and R. Redner, Phys. Chem. Chem. Phys. **7**, 1990 (2005).
[22] K. Rosciszewski, B. Paulus, P. Fulde, and H. Stoll, Phys. Rev. B **60**, 7905 (1999).
[23] K. Rosciszewski and B. Paulus, Phys. Rev. B **66**, 092102 (2002).
[24] T. H. K. Barron and C. Domb, Proc. R. Soc. London, Ser. A **227**, 447 (1955).
[25] K. F. Niebel and J. A. Venables, in *Rare Gas Solids*, edited by M. L. Klein and J. A. Venables (Academic Press, London, 1976), Vol. 1, p. 558.
[26] L. Jansen, Adv. Quantum Chem. **2**, 119 (1965).
[27] D. D. Richardson and J. Mahanty, J. Phys. C **10**, 2763 (1977).
[28] V. V. Goldman, J. Phys. C **8**, L119 (1975).
[29] I. A. Harris, R. S. Kidwell, and J. A. Northby, Phys. Rev. Lett. **53**, 2390 (1984).
[30] O. Echt, K. Sattler, and E. Recknagel, Phys. Rev. Lett. **47**, 1121 (1981).
[31] J. Farges, M. F. de Feraudy, B. Raoult, and G. Torchet, J. Chem. Phys. **84**, 3491 (1986).
[32] D. J. Wales, J. P. K. Doye, A. Dullweber, and F. Naumkin, *The Cambridge Cluster Database*, Cambridge (1997); http://www-wales.ch.cam.ac.uk/CCD.html
[33] Y. Xiang, H. Jiang, W. Cai, and X. Shao, J. Phys. Chem. **108**, 3586 (2004).
[34] B. W. van de Waal, G. Torchet, and M. F. de Feraudy, Chem. Phys. Lett. **331**, 57 (2000).
[35] S. I. Kovalenko, D. D. Solnyshkin, and E. T. Verkhovtseva, Low Temp. Phys. **26**, 207 (2000).
[36] S. I. Kovalenko, D. D. Solnyshkin, E. A. Bondarenko, and E. T. Verkhovtseva, J. Cryst. Growth **191**, 553 (1998).
[37] B. W. van de Waal, J. Cryst. Growth **158**, 153 (1996).
[38] B. W. van de Waal, Phys. Rev. Lett. **76**, 1083 (1996).
[39] J. P. K. Doye and F. Calvo, Phys. Rev. Lett. **86**, 3570 (2001).
[40] J. P. K. Doye and F. Calvo, J. Chem. Phys. **116**, 8307 (2002).
[41] H. R. Glyde, in *Rare Gas Solids*, edited by M. L. Klein and J. A. Venables (Academic Press, London, 1976), Vol. 1, p. 382.
[42] R. Brühl, R. Guardiola, A. Kalinin, O. Kornilov, J. Navarro, T. Savas, and J. P. Toennies, Phys. Rev. Lett. **92**, 185301 (2004).
[43] E. Kim and M. H. W. Chan, Science **305**, 1941 (2004).
[44] F. Calvo, J. P. K. Doye, and D. J. Wales, J. Chem. Phys. **114**, 7312 (2001).
[45] R. Specchio, A. Famulari, and M. Raimondi, J. Mol. Struct.: THEOCHEM **549**, 77 (2001).
[46] S. M. Cybulski and R. R. Toczylowski, J. Chem. Phys. **111**, 10520 (1999).
[47] F. M. Tao, J. Chem. Phys. **111**, 2407 (1999).
[48] J. E. Jones, Proc. R. Soc. London, Ser. A **106**, 709 (1924).
[49] A. Kratzer, Z. Phys. **3**, 289 (1920).
[50] W. Press, S. Teuklosky, W. Vetterling, and B. P. Flannery, *Numerical Recipes in Fortran 77* (Cambridge University Press, New York, 1992).
[51] G. Moyano, M. Pernpointner, and P. Schwerdtfeger, Computer code MAMBO: a multitask simulated annealing many-body potential program for the optimization of clusters, Massey University, Auckland, 2004.
[52] P. Schwerdtfeger, Computer code SAMBA: a solid-state approach using a many-body ansatz, Massey University, Auckland, 2004.
[53] R. C. Weast and M. J. Astle, *CRC Handbook*, 82nd ed. (CRC Press, Boca Raton, FL, 2001).
[54] M. Douglas and N. M. Kroll, Ann. Phys. (N.Y.) **82**, 89 (1974).
[55] B. A. Hess, Phys. Rev. A **33**, 3742 (1986).
[56] T. H. Dunning, J. Chem. Phys. **90**, 1007 (1989). See also http://www.emsl.pnl.gov

[57] A. K. Wilson, D. E. Woon, K. A. Peterson, and T. H. Dunning, J. Chem. Phys. **110**, 7667 (1999).
[58] D. E. Woon and T. H. Dunning, J. Chem. Phys. **98**, 1358 (1993).
[59] S. F. Boys and F. Bernardi, Mol. Phys. **19**, 553 (1970).
[60] M. Ross, J. Chem. Phys. **73**, 4445 (1980).
[61] V. F. Lotrich and K. Szalewicz, J. Chem. Phys. **106**, 9688 (1997).
[62] O. Novaro, Pol. J. Chem. **72**, 1432 (1998).
[63] B. Paulus, K. Rosciszewski, N. Gaston, P. Schwerdtfeger, and H. Stoll, Phys. Rev. B **70**, 165106 (2004).
[64] M. Grimsditch, P. Loubeyre, and A. Polian, Phys. Rev. B **33**, 7192 (1986).
[65] F. H. Ree and C. Bender, Phys. Rev. Lett. **32**, 85 (1974).
[66] C. A. Parish and C. E. Dykstra, J. Chem. Phys. **101**, 7618 (1994).
[67] A. R. Janzen and R. A. Aziz, J. Chem. Phys. **107**, 914 (1997).
[68] R. A. Aziz and M. J. Slaman, Chem. Phys. **130**, 187 (1989).
[69] R. J. Gdanitz, Chem. Phys. Lett. **348**, 67 (2001).
[70] K. Leonhard and U. K. Deiters, Mol. Phys. **98**, 1603 (2000).
[71] E. Ermakova, J. Solca, G. Steinebrunner, and H. Huber, Chem.-Eur. J. **4**, 377 (1998).
[72] R. A. Aziz, J. Chem. Phys. **99**, 4518 (1993).
[73] P. Slavícek, R. Kalus, P. Paska, I. Odvárková, P. Hobza, and A. Malijevsky, J. Chem. Phys. **119**, 2102 (2003).
[74] G. Marcelli and R. J. Sadus, J. Chem. Phys. **112**, 6382 (2000).
[75] J. A. Barker and A. Pompe, Aust. J. Phys. **21**, 1683 (1968).
[76] T. P. Haley and S. M. Cybulski, J. Chem. Phys. **119**, 5487 (2003).
[77] G. Marcelli and R. J. Sadus, J. Chem. Phys. **112**, 6382 (2000).
[78] R. A. Aziz and M. J. Slaman, Mol. Phys. **58**, 679 (1986).
[79] J. O. Hirschfelder, C. F. Curtiss, and R. B. Bird, *The Molecular Theory of Gases and Liquids* (Wiley, New York, 1964).
[80] N. W. Ashcroft and N. D. Mermin, *Solid State Physics* (Saunders College Publishing Philadelphia, 1976).
[81] J. E. Lennard-Jones and A. E. Ingham, Proc. R. Soc. London, Ser. A **107**, 636 (1925).
[82] B. G. Kane and M. Goeppert-Mayer, J. Chem. Phys. **8**, 642 (1940).
[83] T. Kihara and S. Koba, J. Phys. Soc. Jpn. **7**, 348 (1952).
[84] H. Cynn, C. S. Yoo, B. Baer, V. Iota-Herbei, A. K. McMahan, M. Nicol, and S. Carlson, Phys. Rev. Lett. **86**, 4552 (2001).
[85] A. K. McMahan, Phys. Rev. B **33**, 5344 (1986).
[86] R. A. Guyer, Solid State Phys. **23**, 413 (1969).
[87] E. Lombardi and L. Jansen, Phys. Rev. **167**, 822 (1968).
[88] H. Shimizu, H. Tashiro, T. Kume, and S. Sasaki, Phys. Rev. Lett. **86**, 4568 (2001).
[89] Y. Endoh, G. Shirane, and J. Skalyo, Jr., Phys. Rev. B **11**, 1681 (1975).
[90] J. Skalyo, Jr., Y. Endoh, and G. Shirane, Phys. Rev. B **10**, 3647 (1975).
[91] N. A. Lurie, G. Shirane, and J. Skalyo, Jr., Phys. Rev. B **9**, 5300 (1974).
[92] S. Gewurtz and P. Stoicheff, Phys. Rev. B **10**, 3487 (1974).
[93] F. Y. Naumkin and D. J. Wales, Mol. Phys. **96**, 1295 (1999).
[94] For the helium cluster calculations we used an *ab initio* potential from R. Specchio, A. Famulari, and M. Raimondi, J. Mol. Struct.: THEOCHEM **549**, 77 (2001), fitted to the analytic form of Eq. (2).
[95] R. Grisenti, W. Schöllkopf, J. P. Toennies, G. C. Hegerfeldt, T. Köhler, and M. Stoll, Phys. Rev. Lett. **85**, 2284 (2000).
[96] C. Domb and L. Salter, Philos. Mag. **43**, 1083 (1952).
[97] K. Clemenger, Phys. Rev. B **32**, 1359 (1985).
[98] Y. Fuji, N. A. Lurie, R. Pynn, and G. Shirane, Phys. Rev. B **10**, 3647 (1974).
[99] J. S. Lee, Theor. Chem. Acc. **113**, 87 (2005).
[100] O. G. Peterson, D. N. Batchelder, and R. O. Simmons, Phys. Rev. **150**, 703 (1966).
[101] L. A. Schwalbe, R. K. Crawford, H. H. Chen, and R. A. Aziz, J. Chem. Phys. **66**, 4493 (1977).
[102] I. J. Zucker, J. Phys. A **8**, 1734 (1975).